Wintertime organic and inorganic aerosols in Lanzhou, China: Sources, processes and comparison with the results during summer

J. Xu[1], J. Shi[2], Q. Zhang[3], X. Ge[4], F. Canonaco[5], A. S. H. Prévôt[5, 6], M. Vonwiller[7], S. Szidat[7], J. Ge[2], J. Ma[8], Y. An[1], S. Kang[1], D. Qin[1]

[1]State Key Laboratory of Cryospheric Sciences, Cold and Arid Regions Environmental and Engineering Research Institute, CAS, Lanzhou 730000, China

[2]Key Laboratory for Semi-Arid Climate Change of the Ministry of Education, College of Atmospheric Sciences, Lanzhou University, Lanzhou 730000, China

[3]Department of Environmental Toxicology, University of California, Davis, CA 95616, USA

[4]Jiangsu Key Laboratory of Atmospheric Environment Monitoring and Pollution Control (AEMPC), School of Environmental Science and Engineering, Nanjing University of Information Science & Technology, Nanjing 210044, China

[5]Laboratory of Atmospheric Chemistry, Paul Scherrer Institute (PSI), Villigen 5232, Switzerland

[6]State Key Laboratory of Loess and Quaternary Geology and Key Laboratory of Aerosol Chemistry and Physics, Institute of Earth Environment, Chinese Academy of Sciences, 710075 Xi'an, China

[7]Department of Chemistry and Biochemistry & Oeschger Centre for Climate Change Research, University of Bern, Berne, 3012, Switzerland

[8]College of Earth Environmental Science, Lanzhou University, Lanzhou 730000, China

Correspondence to: J. Xu (jzxu@lzb.ac.cn)

Abstract

Lanzhou, which is located in a steep Alpine valley in western China, is one of the most polluted cities in China during the wintertime. In this study, an Aerodyne high resolution time-of-flight aerosol mass spectrometer (HR-ToF-AMS), a seven-wavelength aethalometer, and a scanning mobility particle sizer (SMPS) were deployed during January 10 to February 4, 2014 to study the mass concentrations, chemical processes, and sources of sub-micrometer particulate matter (PM_1). The average PM_1 concentration during this study was 57.3 μg m^{-3} (ranging from 2.1 to 229.7 μg m^{-3} for hourly averages) with organic aerosol (OA) accounting for 51.2%, followed by nitrate (16.5%), sulphate (12.5%), ammonium (10.3%), black carbon (BC, 6.4%), and chloride (3.0%). The mass concentration of PM_1 during winter was more than twice the average value observed at the same site in summer 2012 (24.5 μg m^{-3}), but the mass fraction of OA was similar in the two seasons. Nitrate contributed a significantly higher fraction to the PM_1 mass in winter compared to summer (16.5% vs. 10%), largely due to more favoured partitioning to the particle phase at low air temperature. The mass fractions of both OA and nitrate increased by ~5% (47% to 52% for OA and 13% to 18% for nitrate) with the increase of the total PM_1 mass loading, while the average sulphate fraction decreased by 6% (17% to 11%), indicating the importance of OA and nitrate for the heavy air pollution events in Lanzhou. The size distributions of OA, nitrate, sulphate, ammonium, and chloride all peaked at ~500 nm with OA being slightly broader, suggesting that aerosol particles were internally mixed during winter, likely due to frequently calm and stagnant air conditions during wintertime in Lanzhou (average wind speed: 0.82 m s^{-1}).

The average mass spectrum of OA showed a medium oxidation degree (average O/C ratio of 0.28), which was lower than that during summer 2012 (O/C = 0.33). This is consistent with weaker photochemical processing during winter. Positive matrix factorization (PMF) with the multi-linear engine (ME-2) solver identified six OA sources, i.e., a hydrocarbon-like OA (HOA), a biomass burning OA (BBOA), a cooking-emitted

OA (COA), a coal combustion OA (CCOA), and two oxygenated OA (OOA) factors. One of the OOAs was less-oxidized (LO-OOA) and the other one of more-oxidized (MO-OOA). LO-OOA was the most abundant OA component (22.3% of OA mass), followed by CCOA (22.0%), COA (20.2%), MO-OOA (14.9%), BBOA (10.8%), and HOA (9.8%). The mass fraction of primary OA (= HOA + BBOA + COA + CCOA) increased during high PM pollution periods, indicating that local primary emissions were a main reason for the formation of air pollution events in Lanzhou during winter. Radiocarbon (^{14}C) measurement was conducted on four $PM_{2.5}$ filter samples from this study, which allowed for a quantitative source apportionment of organic carbon (OC). The non-fossil sources on average accounted for 55 ± 3% of OC which could be mainly from biomass burning and cooking activities, suggesting the importance of non-fossil sources for the PM pollution in Lanzhou. Combining with the PMF results, we also found that a large fraction (66%) of the secondary OC was from non-fossil OC.

1 Introduction

Frequent haze pollution events in urban areas in China have been a widespread concern in recent years due to its high adverse health effects, visibility degradation and climate effects (Chan and Yao, 2008). The Chinese Central Government had put in extensive efforts to find urgent and suitable control strategies to reduce further deterioration of air quality. Strategies such as promoting energy conservation and emission reduction measures and new air quality standards ($PM_{2.5}$ currently *vs*. PM_{10} in the past) have been implemented in the last three years (http://www.gov.cn/zwgk/2013-09/12/content_2486773.htm). Many local governments have also launched measures such as shutting down some highly polluting factories and restricting the use of private vehicles to reduce air pollution in their cities. However, air pollution in China is still far from being controlled due to its complex sources and limited knowledge on the multiple pathways leading to secondary aerosol formation and dynamic variation of aerosol mass loading.

Lanzhou, the capital of Gansu province, is located at the northwest of China and has experienced air pollution issues since the 1960s due to emissions from the petrochemical industry and its valley terrain which tended to form stagnant meteorological conditions (Tang et al., 1985; Zhang et al., 2000). Air pollution is still serious and has become more variable in recent years (since 2000) because of fast urbanization and increased energy consumption. The severity of air pollution often reaches maximum intensity during winter due to coal combustion for domestic heating and cooking, similar to the situations in most cities of northern China (Wang et al., 2014). Despite the serious air pollution during winter in Lanzhou, aerosol chemistry, sources, and formation and transformation processes were poorly documented in the literature, which limit the development and implementation of efficient control strategies.

The chemical and physical properties of atmospheric aerosol particles during winter, especially during haze episode, have been recently investigated in metropolitan cities in Eastern China (Sun et al., 2006; Zhao et al., 2013; Huang et al., 2014; Sun et al., 2014). For example, the mean aerosol optical depth at 500 nm were up to ~0.7 during the month-long heavy haze pollution episode during January 2013 in Beijing (Bi et al., 2014); The airborne microbes were found in particulate matter (PM) during hazy period which may potentially include respiratory microbial allergens and pathogens (Cao et al., 2014). Collection and analysis of filter samples have enabled quantification of the chemical composition of PM using a suite of off-line instruments (such as ion chromatography, organic and element carbon analyzer, inductively coupled plasma-mass spectrometry and so on) in the laboratory (He et al., 2001; Zheng et al., 2005; Sun et al., 2006; Sun et al., 2011a; Zhang et al., 2013; Zhao et al., 2013), but often incapable of capturing details of the atmospheric evolution processes during the typical lifecycle of aerosol.

Previous studies on source apportionment of aerosol particle identified dust, traffic, industry, cooking-related activities, and secondary formation as important contributors, although the contributions of individual sources may change drastically with location,

season, and different apportionment algorithms (Zheng et al., 2005; Yu et al., 2013; Huang et al., 2014). For example, Zheng et al. (2005) used chemical mass balance (CMB) receptor model to quantitatively apportion the sources that contribute to fine PM concentration in Beijing and found coal combustion contributed 16% of fine PM mass in January. By contrast, principal component analysis of the same dataset estimated almost twice amount of aerosols from coal combustion (Song et al., 2006). Source apportionment techniques, such as the positive matrix factorization (PMF) allow us to use thousands of fragment ions for source identification and use the real measurement uncertainties to constrain the fitting, and would thus appear more suitable to identify and apportion PM to their sources (Ulbrich et al., 2009). Compared with the number of aerosol source apportionment studies using PMF in Eastern China (e.g., Sun et al., 2013b; Zhang et al., 2013), there were fewer studies in inland cities of China (Elser et al., 2016), the results of which can be used for inter-comparison and understanding the difference of aerosol pollution in different parts of China. In addition, it has been known that a large mass fraction of ambient PM during haze episodes is from fine particles, of which secondary species (some carbonaceous components, sulphate, nitrate, and ammonium) are major components (Zhao et al., 2013). However, the formation and evolution mechanisms of those secondary species were poorly understood, and previous models tended to underestimate the secondary species budget in polluted regions (e.g., Volkamer et al., 2006; Carlton et al., 2010; Hodzic et al., 2016).

Online instruments based on mass spectrometric techniques, such as Aerodyne aerosol mass spectrometer (AMS) (Jayne et al., 2000), have advantages on probing the fast aerosol chemical processes because of the instrument can output data with a large amount of chemical information and its fine time resolution (in minutes) and mass sensitivity (in ng m^{-3}) (Canagaratna et al., 2007). Aerodyne high resolution time-of-flight mass spectrometer (HR-ToF-AMS) have been widely employed for the chemical characterization of submicron aerosol (PM_1) (DeCarlo et al., 2006), which provides on-line quantitative mass spectra of the non-refractory (inorganic and organic) aerosol components with high time resolution. Frequently, the organic aerosol (OA) can be

143 further analyzed using the PMF algorithm (Ulbrich et al., 2009; Zhang et al., 2011a),
144 which can represent the organic mass spectral matrix as a set of source/process-related
145 factor mass spectra and time series. In addition, carbon isotope technique has been
146 recently applied to quantify the fossil/non-fossil origins of carbonaceous aerosols, and in
147 combination with AMS-PMF analyses, the assessment of the origin of secondary organic
148 aerosol (SOA) became possible (Minguillon et al., 2011; Huang et al., 2014; Zotter et al.,
149 2014; Beekmann et al., 2015).

150

151 In a previous study, we used an HR-ToF-AMS to investigate the chemical characteristics
152 of PM_1 in the urban area of Lanzhou during summer 2012 (Xu et al., 2014). During that
153 study, organics in PM_1 was found to mainly originate from traffic, cooking activities, and
154 chemical reactions which produced semi-volatile and less-volatility oxygenated OA.
155 Compared to summer situation, energy consumption for heating is huge during winter
156 and the dry and stable meteorological condition in the valley leads to longer aerosol
157 lifetime during winter. Thus aerosols are influenced largely by very different
158 meteorological conditions and chemical processes between the two seasons. More
159 intensive measurements of PM chemical characteristics are needed to better understand
160 aerosol sources, to quantify their lifetime in the atmosphere and to constrain the
161 uncertainties of their climatic influences. During winter of 2013/2014, we conducted such
162 a study at an urban site of Lanzhou. In this paper, we focus on the chemical speciation of
163 PM_1 and source apportionment of OA.

164

165 **2 Measurement and methods**

166 2.1 Sampling site

167 Aerosol particle measurements were conducted from January 10 to February 4, 2014, at
168 the top floor of a twenty-two story building (~70 m a.g.l) (36.05°N; 103.85°W, 1569 m
169 a.s.l) in the campus of Lanzhou University (Fig. S1a). The campus is located in the
170 Chenguan district of Lanzhou which is a cultural and educational area. The twenty-two
171 story building sits at the western edge of the campus and faces a south-northern arterial

road (Fig. S1a). At the campus side of this building, there is a three story dining hall of Lanzhou University, and over the arterial road side, there are many restaurants and residents. The room temperature was kept at ~20 °C by a central heating radiator. The weather in Lanzhou during the campaign was cold (avg. T = 0.5 °C) and dry (avg. RH = 28%), and was influenced by the Asian winter monsoon. Because Lanzhou is surrounded by mountains, atmospheric condition is normally stable with low wind speed (on average 0.82 m s^{-1} during this study). The sampling site represents a typical urban area dominated by residential and commercial area.

2.2 Instruments

The physiochemical properties of aerosol particles were monitored in real-time by a suite of instruments (Fig. S1b). The sampling inlet, constructed using 0.5 inch copper tube, stemmed out of the rooftop by about 1.5 m. A $PM_{2.5}$ cyclone (model URG-2000-30EH, URG Corp., Chapel Hill, NC, USA) was used for removing coarse particles. The length of the sampling line was about 5 m. A diffusion dryer was placed upstream of this line to eliminate potential RH effect on particles. The inlet was shared by an Aerodyne HR-ToF-AMS (Aerodyne, Inc., Billerica, MA, USA) for the size-resolved chemical speciation of non-refractory sub-micrometer PM (NR-PM_1), a single particle intra-cavity laser induced incandescence photometer (SP2, DMT, Inc., Boulder, CO, USA) for refractory black carbon (rBC) measurement, a customer-made scanning mobility particle sizer (SMPS) (Wiedensohler et al., 2012) for measuring particle size distribution between 10-800 nm, and a 7-λ aethalometer (model AE31, Magee Scientific, Berkeley, CA, USA) to derive the mass concentration of light absorbing black carbon (BC) particles. The total air flow rate from the inlet was ~ 16 L min^{-1}, with a vacuum pump drawing the air at a flow rate of 10 L min^{-1} and the other 6 L min^{-1} sampled by the instruments. The retention time of particles in the sampling line was less than 2.5 s. A parallel inlet with a 1:10 dilution stage was setup for real-time $PM_{2.5}$ measurement using a tapered element oscillating microbalance (TEOM series 1400a, R&P, East Greenbush, NY, USA). The roof of the building also hosted instruments for monitoring meteorological parameters such as

visibility, air temperature, wind direction, wind speed, and RH. The visibility was measured with a LED-based (880 nm) forward (42°) scattering visibility sensor (model M6000, Belfort Ins., Maryland, USA).

2.2.1 HR-ToF-AMS operation

A detailed description of the principle and design of HR-ToF-AMS can be found elsewhere (Jayne et al., 2000; DeCarlo et al., 2006). Briefly, HR-ToF-AMS consists of three major sections: the inlet system, the particle sizing vacuum chamber, and the particle composition detection section. The combination of a 100 μm orifice and an aerodynamic lens in the inlet system are used to focus the airborne particles into a concentrated and narrow beam, and then accelerated into the vacuum chamber (~10^5 Torr) modulated by a chopper for measuring aerodynamic size of the particle; Before being detected, the particles are flash vaporized under 600 °C and ionized by a 70 eV electron impact, and finally detected by the high resolution time-of-flight mass spectrometer. The chopper works at three positions alternately, i.e., an open position which transmits the particle beam continuously, a close position which blocks the particle beam completely, and a chopping position which modulates the beam transmission (2% duty cycle). The open and close positions yield the bulk and background signals for the airborne particle, respectively, while the chopping position modulates the particle beam by spinning chopper wheel (~150 Hz) to yield size-resolved spectral signals. The mass spectrometer in the detection section works in two modes based on the shape of the ion path, i.e., V-mode and W-mode, with high sensitivity and high chemical resolution (~6000 m/Δm), respectively. The highly sensitive V-mode signals are usually used for reporting mass concentration, while the high chemical resolution W-mode signals are used for the analyses of mass spectrum. The time resolution for both V and W modes was 5 min. Under V-mode, the instrument switched between the mass spectrum mode and the PToF mode every 15 s, spending 6 and 9 s on each, and cycled 20 times in one run; No PToF data were recorded in W-mode due to low signal-to-noise (S/N) ratios.

The instrument was calibrated for ionization efficiency (IE), inlet flow rate, and particle sizes using the standard procedure described by (Jayne et al., 2000). For example, the size calibration was performed following the general protocol used in the AMS community. We used standard polystyrene latex (PSL) spheres (Duke Scientific Corp., Palo Alto, CA) (100-700nm) and mono-dispersed ammonium nitrate particles (100-300nm), respectively. These three calibrations were performed at the beginning, in the middle and end of the field study. Particle-free ambient air was sampled at the end of the study to determine the detection limits (DLs) of individual species and also for adjusting the fragmentation table. Note that since no in-situ measurement of gas phase CO_2, the subtraction of a constant CO_2 signal (400 ppm based on filtered-air measurement in this study) may introduce uncertainties in the quantification of the organic-CO_2^+ signal. However, this artifact was expected to be small (less than 5% error in organic-CO_2^+ quantification) due to the high OA concentration (Xu et al., 2014). Default relative ionization efficiency (RIE) values were assumed for organics (1.4), nitrate (1.1), sulphate (1.2), and chloride (1.3), while an RIE value of 3.9 was determined for ammonium following the analysis of pure NH_4NO_3. The close concentrations between measured ammonium and predicted ammonium based on the stoichiometric charge balance between nitrate, sulphate, and chloride (slope = 0.94, Fig. S4) suggest that these RIE values are suitable for this campaign.

2.2.2 Operations of other instruments

The SMPS consisting of a condensation particle counter (CPC) (TSI, model 3772) and a differential mobility analyser (DMA) was deployed at 5 min interval. Sample and sheath flow rates of the DMA were set to 1 L min^{-1} and 5 L min^{-1}, respectively. The SMPS was calibrated using a polystyrene latex (PSL) standard prior to field measurements.

The SP2 uses an intra-cavity Nd:YAG laser at 1064 nm to determine the light scattering and laser-induced incandescence of individual rBC (namely material associated with a strongly absorbing component at 1064 nm). The SP2 incandescence signal was used to

obtain single particle rBC mass after calibration with Aquadag standard BC particles. The measured rBC mass is converted to a mass equivalent diameter, which is termed as the BC core diameter (D_c) - the diameter of a sphere containing the same mass of rBC as measured in the particle. Any measured particle with a detectable incandescence signal is referred to as an rBC particle, whereas a particle which only exhibits a scattering signal is termed as a non-BC particle. The total rBC mass loading is reported as the sum of all detected single particle rBC masses.

The aethalometer measures the optical attenuation (absorbance) of light from LED lamps emitting at seven wavelengths (370, 470, 520, 590, 660, 880, and 950 nm) with a typical half-width of 20 nm. The difference in light transmission through the particle-laden sample spot and a particle free reference spot of the filter is attributed to the absorption caused by aerosol. The attenuation of light is converted to the BC mass concentration using wavelength-dependent calibration factors as recommended by the manufacturer. BC was measured using data at 880 nm using a specific attenuation cross section of 16.6 $m^2\ g^{-1}$ during the campaign. The flow rate was maintained at 4.8 L min^{-1} calibrated using a flow meter. Detection limit of the aethalometer BC was determined to be 0.16–0.28 μg m^{-3} with a flow rate of 4.8 LPM and 5 min time interval, calculated as three times the standard deviation (3σ) of the dynamic blanks. The TEOM was operated at a temperature of 40 °C other than normal operation condition (50 °C) to dry the aerosol in order to minimize mass loss due to volatilization of semi-volatile aerosol compounds. The time resolution of $PM_{2.5}$ mass concentration was 5 min.

2.3 Data processing

2.3.1 General AMS data processing

The HR-ToF-AMS data were processed using the standard software of SQUIRREL (v1.56) and PIKA (v1.15c) (http://cires.colorado.edu/jimenez-group/ToFAMSResources/ToFSoftware/index.html) to determine the mass concentrations and the size distributions of the NR-PM_1 species and the ion-speciated

mass spectra of organics, written in IGOR (Wavemetrics, Inc., Lake Oswego, OR, USA). An empirical particle collection efficiency (CE) of 0.5 was used, which has been widely used in field studies employing AMS with a dryer installed in front of the equipment's particle inlet. This CE value was further validated by the consistency and reasonable slope between HR-ToF-AMS measured mass concentrations and SMPS-determined particle volumes (section 3.1.2, R^2 = 0.9, slope = 1.48). The elemental ratios of OA (O:C, H:C, and OM:OC) for this study was determined using the "Aiken ambient" method (Aiken et al., 2008) other than the "improved-ambient" method (Canagaratna et al., 2015) which increased O:C on average by 27%, H:C on average by 10%, and OM:OC on average by 7% (Fig. S2). These "Aiken ambient" results of elemental ratios are more suitable here to allow for comparison with those during summer 2012.

2.3.2 Positive Matrix Factorization (PMF) analyses

The source decomposition of organics was analysed by PMF with the multilinear engine (ME-2) algorithm which serves to reduce rotational ambiguity within the PMF2 algorithm. The ME-2 algorithm allows the user to add a priori information into the model (e.g., source profiles) to constrain the matrix rotation and separate the mixed solution or the weak solution. The PMF analysis of organic matrix using ME-2 algorithm is implemented within the toolkit SoFi (Source Finder) and perform by the so-called a-value approach (Canonaco et al., 2013). First, organic matrix was analysed using the PMF2.exe algorithm in robust mode (Paatero and Tapper, 1994) and explored using the PMF Evaluation Toolkit (PET) (Ulbrich et al., 2009). The PMF solution was evaluated following the procedures outlined in Table 1 of Zhang et al. (2011a) including modification of the error matrix and downweight of low S/N ions. Moreover, based on the AMS fragmentation table, some organic ions were not directly measured but scaled to the organic signal at *m*/*z* 44, which were downweighted by increasing their errors by a factor of 3. Some highly polluted periods were deleted during PMF analysis such as January 22-23, 2014. The results of four, five, and six factor solutions with *f*Peak at 0 are shown in supplementary material (Fig. S5-S7). It is easy to find that a coal combustion-

emitted OA (CCOA) factor, a cooking-emitted OA (COA) factor, a less-oxidized and more-oxidized OA (LO-OOA and MO-OOA) factors could be clearly separated in the four-factor solution; for the CCOA factor, there were significant contributions from *m*/*z* 55, 57, 60, 73, 91, and 115 in the mass spectrum, suggesting a mixing of multiple sources. In the five-factor solution, a hydrocarbon-like OA (HOA) factor was separated; however, *m*/*z* 60 and 73 which are related to biomass burning OA (BBOA) could not be separated. We then performed OA source apportionment using the ME-2 algorithm by constraining the profiles of HOA and BBOA with the fixed a-value of 0.1 for HOA and 0.4 for BBOA. The a-value test was performed following the technical guidelines presented in Crippa et al. (2014). The reference profile of HOA was adopted from the HOA of the summer study and the reference profile of BBOA was adopted from the nine-factor PMF solution of this study.

The size distributions of individual OA factors were determined via a multivariate linear regression technique (Ge et al., 2012). This algorithm assumes that each OA mass spectrum is the linear superposition of the mass spectra of individual OA factors, whose mass profiles are constant across the whole size range. Further details about the algorithm can be found in Xu et al. (2014).

2.3.3 Radiocarbon (^{14}C) data analysis

In order to identify the origins of SOA, we conducted ^{14}C analysis on four filter samples. These filter samples were collected at the CAEERI site which is about 500 m away from the LZU site (Fig. S1a). Filter samples were collected using a low volume $PM_{2.5}$ sampler (16.7 L min^{-1}) during January 2014 with a 24 h sampling time in every week for each filter (January 3rd, 8th, 15th, and 23rd, respectively) on pre-baked quartz filters. One field blank filter was collected and analysed to correct the filter sample measurements. Here, we use the results of these four filter samples to roughly represent the average situation of the field sampling because of the relative stable meteorological conditions (section 3.1.1) and similar aerosol sources during the field study (section 3.1.3). Due to

the limitation of the small amount of filter samples, the results based on this carbon isotopic data are preliminary and comprehensive validation is an ongoing work. Organic carbon (OC) was separated from the filters by combustion at 375 °C during 200s in pure oxygen in a thermo-optical OC/EC analyser (Model 4L, Sunset Laboratory Inc, USA) (Zhang et al., 2012). The carbon isotopic analysis was conducted by online coupling of the OC/EC analyser with the accelerator mass spectrometry system MICADAS at the University of Bern, Switzerland (Zotter et al., 2014; Agrios et al., 2015). Fossil ^{14}C measurement results were transferred into the non-fossil fraction (f_{NF}) of OC using a conversion factor of 1.03 (Zhang et al., 2015b).

For the apportionment of AMS-PMF OA factors using ^{14}C data (Zotter et al., 2014), we assume that all OC sources are represented by the six PMF factors and the f_{NF} in NR-PM_1 was the same as that in $PM_{2.5}$. The OA mass of each PMF factor and total OA were first converted to OC mass using the OM:OC ratios derived from its MS ($OM:OC_{HOA}$ = 1.29, $OM:OC_{BBOA}$ = 1.5, $OM:OC_{COA}$ = 1.27, $OM:OC_{CCOA}$ = 1.37, $OM:OC_{LO\text{-}OOA}$ = 1.55, $OM:OC_{MO\text{-}OOA}$ = 2.01, $OM:OC_{total}$ = 1.51). For the OC mass concentration of the AMS factors, the following notations, hydrocarbon-like organic carbon (HOC), biomass burning organic carbon (BBOC), cooking organic carbon (COC), coal combustion organic carbon (CCOC), oxygenated organic carbon (OOC), total organic carbon from AMS (TOC_{AMS}), were adopted in the following sections. An f_{NF} value was assumed a priori for the primary PMF factors HOC, BBOC, COC, and CCOC. The average f_{NF} of OOC is then derived by the equation below:

$$f_{NF\_OOC} = (TOC_{NF\_AMS} - f_{NF\_HOC} \times HOC - f_{NF\_BBOC} \times BBOC - f_{NF\_COC} \times COC - f_{NF\_CCOC} \times CCOC) / (SV\text{-}OOC + LV\text{-}OOC)$$

Here HOC is assumed to originate from gasoline and diesel exhaust and contains exclusively of fossil carbon, i.e., f_{NF_HOC} = 0; BBOC is estimated to be originated from biomass burning, i.e., f_{NF_BBOC} = 1; COC is assumed to originate from non-fossil carbon

such as cooking oil and dressing, i.e., $f_{NF\_COC} = 1$; CCOC is estimated to originate from coal combustion, i.e., $f_{NF\_CCOC} = 0$.

3 Results and discussions

3.1 Overview of field study

3.1.1 Meteorological conditions

Fig. 1 shows the time series of meteorological parameters and PM_1 components during the campaign. The measurement site mainly received air masses from northern and northeastern associated with low wind speeds (WS) ranging from 0.6 to 1.1 m s^{-1} (on daily average: 0.8 ± 0.2 m s^{-1}). The mountains to the north and south of the city could significantly reduce the wind speeds. Air temperature ranged from −5.0 to 6.6 °C (average = 0.6 ± 3.9 °C) for the diurnal variation during the campaign, but had an evident increase after the Chinese New Year (January 31, 2014) (Fig. 1a). No precipitation event occurred during the campaign, and RH was pretty low ranging from 16.8 to 39.5% (on daily average = 27.5 ± 7.4%) for the diurnal variation. Overall, the meteorological conditions during the campaign were much stable and dryer than those during summer 2012 (on average: 1.2 ± 0.6 m s^{-1} for WS and 60 ± 17 % for RH).

3.1.2 Inter-comparisons

The inter-comparisons between AMS *vs*. SMPS and TEOM are shown in Fig. S3. Comparison between the mass concentration of PM_1 and the volume of particle measured by SMPS is tightly correlated (R^2 = 0.9) with a slope of 1.48, which represents the average density of bulk particles, assuming that the AMS and the SMPS measure a similar particle population. This value is indeed very close to the estimated PM_1 density (1.46) based on the measured particle composition for this study (using density of 1.2 g m^{-3} for organics, 1.72 g m^{-3} for NH_4NO_3, 1.77 g m^{-3} for $(NH_4)_2SO_4$, 1.52 g m^{-3} for NH_4Cl and 1.8 g m^{-3} for BC) (Zhang et al., 2005; Bond and Bergstrom, 2006). The mass concentration of PM_1 is also closely correlated (R^2 = 0.71) with TEOM $PM_{2.5}$

concentrations with a slope of 0.73. Similar contribution of PM_1 to $PM_{2.5}$ were also observed in other cities in China during winter (Elser et al., 2016), such as Beijing (0.74 during 2011) (Sun et al., 2013b). Note that the actual mass ratio between PM_1 and $PM_{2.5}$ should be higher than these values since refractory materials such as crustal components were not measured.

3.1.3 PM_1 composition, variation, and acidity

The average mass concentration of PM_1 (NR-PM_1 + BC) was 57.3 μg m^{-3} (ranging from 2.1 to 229.7 μg m^{-3} for hourly average) during this study, with 51.2% of organics, 16.5% of nitrate, 12.5% of sulphate, 10.3% of ammonium, 6.4% of BC, and 3.0% of chloride (Fig. 2a). The average mass concentration was more than twice the average value observed during summer 2012 (24.5 μg m^{-3}). All species showed similar day-to-day variation with nitrate being the most significant one (Fig. 1e), suggesting an important local source for nitrate. The mass contributions of PM_1 species from low to high PM_1 concentrations showed an increased contribution for organics (49% to 53%) and nitrate (13% to 18%), but a decreased contribution for sulphate (17% to 11%) and BC (7.3% to 5.3%) suggesting somewhat different chemical processes/sources for each species during the haze pollution (Fig. 2b). Specifically, the increased organics was mainly due to the contribution of primary OA (POA) based on PMF analysis (more discussion are given in section 3.5). During the late part of Chinese New Year holiday (February 3 to end of the study), PM_1 concentration decreased in association with increased wind speed (~1 m s^{-1} to 2 m s^{-1}). NR-PM_1 appeared to be neutralized throughout this study, as indicated by an overall stoichiometric charge balance between the anions (i.e., nitrate, sulphate, and chloride) and the cation ammonium (slope = 0.94, Fig. S4). This result indicates that the inorganic particulate species were mainly present in the forms of NH_4NO_3, $(NH_4)_2SO_4$, and NH_4Cl in PM_1.

3.1.4 Size distribution

The average chemically-resolved size distributions of NR-PM_1 species are shown in Fig. 3a. While all components peaked between 400–500 nm, organic aerosol presented a wider distribution than the inorganics and extended to ~250 nm, suggesting the influence of fresh organics (POA, more discussion are given in section 3.4). These features were similar to those found in most urban sites by the AMS. The similar mode size of inorganics and SOA (Fig. 3c) suggested the well internally mixed air mass during the sampling period. The mass contributions of chemicals at the major peak (400–500 nm) were organics (~50%), nitrate (~20%), ammonium (~15%), sulphate (~10%), and chloride (~5%); while the contribution of organics increased with the decreasing of size mode (Fig. 3c). Comparing with the results observed during 2012 summer, the size distributions of aerosol particle during winter were narrower, although the mode sizes of major peaks were similar, indicating highly mixed and aged aerosol particles during winter. Note that chloride also showed a wider distribution which was more similar with organics other than sulphate and nitrate. This was not observed during 2012 summer and could be related with OA emitted from coal combustion and biomass burning during wintertime. Note that chloride also showed a wider distribution which was more similar with organics other than sulphate and nitrate. This was not observed during 2012 summer and could be related with OA emitted from coal combustion and biomass burning during wintertime.

3.2 Diurnal variations of aerosol species

All species show significant diurnal variations during the study suggesting the important local and regional sources of aerosol (Fig. 4). The observed diurnal trends of BC presented two dominant peaks with one at late morning (10:00–12:00) and another at early evening (20:00–22:00). The morning peak did not overlap with the rush hours (7:00–9:00), different than that of summer 2012; the BC mass loading started to increase from 6:00 continuously during morning, and reached maximum between 10:00–12:00 and then dropped down after the noon time. Another combustion tracer, carbon monoxide

(CO), also showed the similar morning peak (Fig. 5). This morning peak was likely resulted from the contribution of multiple combustion sources, such as coal combustion, biomass burning, and traffic emission which had different morning peaks (see section 3.4), and the formation of inversion layer during winter at Lanzhou which promoted accumulation of air pollutants from enhanced human activities in the morning. This inversion layer frequently formed from night time and diffused after the noon time due to the valley terrain (Zhang et al., 2011b). The temperature profile observed at the suburban Lanzhou (Yuzhong, ~30 km from the sampling site) showed a strong inversion in the low boundary layer during the morning time (Fig. S8). But such influences should be further verified in the future with simultaneous measurements from boundary layer heights. The evening peak of BC could result from increased human activities such as traffic, cooking, and heating coupled with low boundary layer after sunset. Organics had two sharp peaks at the noon time (12:00–13:00) and early evening (19:00–20:00) which correspond to lunch time and dinner time, respectively, indicating the importance of cooking-related emissions of OA. PMF analysis show that cooking-emitted aerosol could contribute up to 50% of organics during meal times (section 3.4.3).

Sulphate presented two peaks with one occurring at the noon time (11:00–14:00) in accordance with the photochemical processes; this peak is narrower than that during summer, likely due to relatively weak photochemical activities. Another minor peak occurred between 20:00–22:00 which was likely due to the lowered boundary layer depth. The significantly higher concentration of sulphate during winter than summer could result from a higher amount of precursor SO_2 emission, wintertime hydroxyl radical formation, and the increased aerosol particle surface due to high PM loadings that facilitated the heterogonous conversion of SO_2 to sulphate (Yong et al., 2012; Pusede et al., 2015; Zheng et al., 2015). The diurnal pattern of sulphate during winter was similar to that of summer 2012 at Lanzhou and summer 2011 at Beijing, but was different from that of Beijing during winter 2011/2012 where aqueous processing was found to could play an important role (Sun et al., 2013b). Chloride had similar diurnal pattern with sulphate, although the evening peak was more obvious. The major source of hydrochloric acid is

biomass burning, coal combustion and waste combustion (Ianniello et al., 2011). The significant evening peak could be related with these sources coupled with the shallow boundary layer. The high background concentrations of chloride during day and night suggest a persistent emission of hydrochloric acid which could be from the heating factory and power plants. The diurnal pattern of chloride during winter was different from that during summer 2012 which peaked during the night time due to temperature-dependent gas-particle partitioning. Nitrate peaked between 12:00–16:00, right after the peak of sulphate. The formation of nitrate during afternoon suggests that nitrate was dominated by the homogeneous photochemical production. Fig. 5 shows the variations of NO_x and O_3 calculated from data downloaded from one station monitored by the Ministry of Environmental Protection of China, ~3 km southwest of sampling site (Fig. S1a); NO had a morning peak (7:00–10:00) and an evening peak (19:00–21:00) corresponding to rush hours; NO_2 increased from 10:00 which formed from NO consumed by O_3 and slightly decreased from 14:00 to 18:00 corresponding to the photolysis of NO_2 and the formation of nitric acid during afternoon. The diurnal change of NO_x (ΔNO_x) mixing ratio was ~50 ppbv (from 150 to 100 ppbv), while the diurnal change of the sum of ΔO_3 and ΔNO_3^- was ~30 ppbv. Considering the higher mixing layer height during afternoon, it seems that nitrate was mainly formed from the photochemical processing of NOx. The diurnal pattern of nitrate during winter was vastly different from that during 2012 summer which was mainly controlled by the dynamic of mixing layer and gas-particle partitioning.

3.3 Bulk characteristics and elemental ratios of OA

Table 1 shows the average elemental mass composition and mass contributions of six ion categories to the total organics. Carbon contributed 67% to the organics following by oxygen (23%), hydrogen (9%), and nitrogen (1%); correspondingly, $C_xH_y^+$ dominated the organics by 59%, following by $C_xH_yO_1^+$ (26%), $C_xH_yO_2^+$ (10%), $H_yO_1^+$ (2%), and $C_xH_yN_p^+$ (2%). Compared with the results of 2012 summer, the organics in winter had higher carbon (67% *vs*. 59%) and $C_xH_y^+$ content (59% *vs*. 56%), and lower oxygen

content (23% *vs*. 26%) (Fig. 6c); this suggests that the organics during winter had a higher fraction of primary compounds than those during summer which was likely due to weaker photochemical activities, lower boundary layer height and more emissions from primary sources. The average O/C of organics, an indicator for oxidation state, was 0.28 during this study which was somewhat lower than that of summer 2012 (0.33) (Fig. 6a and b). Photochemical processing of organics during winter appeared to be significantly weaker and shorter than those during summer as shown by the smaller diurnal peak of O/C (Fig. 6d). The diurnal profile of H/C was inversely correlated with that of O/C, and the peaking of organic aerosol concentration usually corresponded to the high H/C ratio and low O/C ratio, indicating the dominant role of primary OA.

3.4 Source apportionment of OA

Source apportionment via PMF with ME2 engine on OA mass spectra resolved six components, i.e., HOA, COA, CCOA, BBOA, LO-OOA, and MO-OOA. Each component has a unique mass spectral pattern, diurnal pattern, and temporary variation which correlated with corresponding tracers such as inorganic species. Two OOA components can be regarded as surrogates of SOA, with MO-OOA for more aged SOA and LO-OOA for fresher SOA; The HOA, BBOA, COA and CCOA components are regarded as POA based on their low O/C ratios and good correlations with primary aerosol tracers (Fig. 7). Comparison with the source apportionment results of summer 2012, the organic sources and chemical processes during winter 2013/2014 were more complex due to the multiple primary sources. Detailed discussion of each factor is given in the following subsections.

3.4.1 HOA

HOA factors had been frequently separated from the OA in urban area due to the emission from traffic and/or other fossil combustion activities (e.g., Sun et al., 2011b; Ge et al., 2012). The diurnal pattern of HOA in winter 2013/2014 of Lanzhou shows two

predominant peaks in the morning (6:00–10:00) and evening (20:00–21:00), respectively (Fig. 5). The peaks were mainly associated with the traffic rush hours and low PBL depth before and after sunset. The relatively low concentration during afternoon was probably due to the high PBL depth as shown by the mass concentration variations of BC. The correlation between HOA and BC was high (R^2 = 0.64, Fig. 7f and Table 2), as a big fraction of BC has been thought to emit from traffic activities. The minimum of HOA concentration, which typically occurred during afternoon or middle night, was still up to ~2 μg m^{-3} suggesting a high background of HOA which is likely due to the stagnant air condition unfavourable for the diffusion of aerosol. The size distribution of HOA showed a mode size of ~200 nm (Fig. 3b) corresponding to the primary emitted aerosol behaviours and HOA could account for ~25% mass of aerosols between 100-300nm (Fig. 3c). The average concentration of HOA during 2013/2014 winter was 2.9 μg m^{-3} accounting for 9.8% of organics (Fig. 8a). This concentration was higher than that of 2012 summer in Lanzhou (2.9 *vs*. 1.8 μg m^{-3}) likely due to the lower PBL during winter and stagnant air conditions. The mass contribution from HOA is similar to the result of 2013 winter at Beijing (9%) which was also the lowest contributor to the total OA (Sun et al., 2013b; Zhang et al., 2014), probably due to more modern vehicles were used in the recent years.

3.4.2 BBOA

BBOA component had been widely observed in USA and European countries during winter due to the traditional wood burning for residential heating (Alfarra et al., 2007). The BBOA component is thought to be less important in China because coal is the major fuel during winter. BBOA could be an important component in China during some special periods. For example, Zhang et al. (2015a) identified a BBOA factor in urban Nanjing, southeast of China, during harvest seasons of summer and autumn because of the burning of straw. The BBOA component has also been identified in some regions in China where the coal resource is scarce. For example, Du et al. (2015) separated a BBOA factor at a rural site of the northern Tibetan Plateau due to the widely usage of cow dung

cake for heating in this region. The BBOA component has also been identified during winter in cities in southern China because of rich wood resource in these regions (He et al., 2011; Huang et al., 2011; Huang et al., 2013). To our knowledge, only three recently papers have reported the identification of a BBOA factor during winter using online measurement in an urban area of northern China (Elser et al., 2016; Hu et al., 2016; Sun et al., 2016). Although the high contribution of non-fossil carbonaceous aerosol was found (Zhang et al., 2015b) and the mass spectra of organic in other cities (such as Beijing) during winter have also significant contributions from *m*/*z* 60 and 73 (Sun et al., 2013b; Zhang et al., 2014), it is difficult to separate the BBOA using general PMF because of its similar temporal variation with CCOA, such as diurnal pattern (Fig. 4). BBOA contributions presented a clear periodic change (Fig. 1), and on average were high during night time and low during daytime (Fig. 5). This trend is consistent with conventional usage of biomass for heating. The time series of BBOA was also closely correlated with BC and chloride (Table 2) due to significant emission of these species from biomass burning. The average mass concentration of BBOA was 3.2 μg m^{-3}, on average contributing 10.8% of the total OA mass for the entire study (Fig. 8a), but could reach up to ~20% during night and down to less than 5% during afternoon (Fig. 8b). This average concentration was close to the results observed at southern Chinese cities such as Jiaxing (~3.9 μg m^{-3}) (Huang et al., 2013), Kaiping (~1.36 μg m^{-3}) (Huang et al., 2011) and Shenzhen (~5.2 μg m^{-3}) (He et al., 2011).

The size distribution of BBOA peaked at ~400nm which is close to accumulation mode (Fig. 3b). This feature could be due to internal mixing or coagulation of particles. The O/C ratio of BBOA is 0.24, which is consistent with the primary BBOA feature (Ortega et al., 2013). The similar O/C and the dominance of an accumulation mode in the size distribution of BBOA were also observed during winter in Fresno, a major city in the Central Valley of California, USA (Ge et al., 2012; Young et al., 2015).

3.4.3 COA

The COA component has been widely identified in urban AMS studies and observational results by other instruments recently, and it is regarded as important source of OA in urban areas (Abdullahi et al., 2013 and references therein). The MS of COA in this study had a major contribution from $C_xH_y^+$ ions (81.6%) with also an important contribution from $C_xH_yO_1^+$ ions (14.7%), similar as those in HOA (81.0% and 13.0%) (Fig. S9). In comparison with the HOA spectrum, COA had a higher *m*/*z* 55 to 57 ratio (2.0 vs. 0.8) (Fig. 7) which had been postulated as a significant indicator for COA (Sun et al., 2011b; Mohr et al., 2012). In the V-shape plot defined by Mohr et al. (2012), which uses *f*55 *vs.* *f*57 after subtracting the contributions from factors of OOA, CCOA, and BBOA (denoted as OOA_CCOA_BBOA_sub, i.e. $f55_{OOA\_CCOA\_BBOA\_sub}$ and $f57_{OOA\_CCOA\_BBOA\_sub}$), the data can be clearly represented with ones during morning close to HOA line and ones during meal times close to COA line (Fig. S10). The MS of COA is highly similar to that of summer 2012 observation (R^2 = 0.76, slope = 0.99, Fig. S11) which was found to resemble closely the COA MS from other locations (Xu et al., 2014). In fact, the COA components were found to be associated with heating of cooking oils rather than burning of meat/food itself, and indeed the COA mass spectra from cooking of different dishes were highly similar (He et al., 2010). The O/C and H/C ratios of COA were 0.07 and 1.73, respectively, suggesting its feature as POA. This O/C ratio was slightly lower (0.07 vs. 0.11) and the H/C was slightly higher than that of 2012 summer (1.73 vs. 1.69). The size distribution of COA was also peaking between 100–200 nm similar to that of HOA (Fig. 3b). The diurnal variation of COA displayed two predominant peaks standing out at lunch time (12:00–13:00) and dinner time (19:00–20:00), respectively (Fig. 5), and a small breakfast peak (~8:00). This pattern was consistent with that of summer 2012 (Fig. 4) which resulted from the consistent routine life during winter and summer. The enhanced COA concentration at dinner time might be mainly due to the low PBL height and the activity of a formal meal with more attendants and longer time than that of lunch. The temporal variation correlated tightly with $C_6H_{10}O^+$ (R^2 = 0.96, Fig. 7d) which has been reported as the high resolution mass spectral markers for ambient COA (Sun et al., 2011b; Ge et al., 2012).

The average contribution of COA to organics was 20.2% (~10–50%) (Fig. 8a) with an average mass concentration of 5.92 μg m^{-3} which was much higher than those of HOA and BBOA. This contribution is similar to those in Beijing during winter (average 19% of OA with a range of 16–30%) (Sun et al., 2013b), Fresno (~19% of OA) (Ge et al., 2012), Barcelona (17% of OA) (Mohr et al., 2012), and Paris (11–17%) (Crippa et al., 2013). This high fraction indicates that COA is an important local source of OA in Lanzhou regardless of clear or hazy periods (section 3.5).

3.4.4 CCOA

A CCOA component had been identified in this study with its MS similar to the OA from coal burning in lab study (Dall'Osto et al., 2013). The MS of CCOA had high signals at *m*/*z* 41, 43, 44, 55, 57, 69, 91 and 115 (dominated by $C_xH_y^+$ ions) (Fig. 7i) (Elser et al., 2016). $C_xH_y^+$ ions in total account for 69.9% of CCOA MS, following by $C_xH_yO_1^+$ (19.2%) and $C_xH_yO_2^+$ (7.1%). The fractions of $C_xH_y^+$ and $C_xH_yO_1^+$ were similar with those in HOA MS (Fig. S9), but the CCOA MS had high signal intensity at *m*/*z* 44 (mainly CO_2^+) which is different from that of HOA (Fig. 7). This high CO_2^+ fraction was also observed in CCOA MS in Changdao island in China during winter (Hu et al., 2013). Wang et al. (2015) suggested this high CO_2^+ signal is from the oxidative transformation of the pyrolysis products during coal burning. Zhang et al. (2008) reported that 48–68% of particulate organic matter from coal combustion aerosol is found in the form of organic acids. The O/C ratio is thus higher than that of HOA (0.20 *vs*. 0.10) with a lower H/C ratio (1.54 *vs*. 1.86). The CCOA also locates in a lower left position in the triangle plot defined by Ng et al. (2010) (Fig. 9a). These features indicate CCOA is a POA factor but is a little more oxygenated than HOA. The time-dependent concentrations of CCOA correlated with BC (R^2 = 0.59) and chloride (R^2 = 0.49) which also correlated well with HOA and BBOA (Table 2). Note that although the similar temporal variations between BBOA and CCOA, the significant differences between their MS (in particular, m/z 91) suggested their different origins. In addition, high PAH signals had been observed in the

CCOA MS, and this is consistent with previous results that the coal combustion could be a dominate source of PAHs in China (Okuda et al., 2006; Sun et al., 2016).The CCOA mass loading remained high from 20:00 to 10:00, slowly decreased to a minimum at 16:00, and then increased from 16:00 to 20:00 (Fig. 5). This diurnal pattern was similar to that of BBOA which were all mainly emitted from heating. The slower decreasing rate during morning and increasing rate during late afternoon for CCOA than those of BBOA could related with wide usage of coal, such as cooking and power plants. In our summer 2012 observation, we also observed OA signals from coal combustion which suggest persistent emitted during the whole year in Lanzhou. The size distribution of CCOA peaked ~450 nm (Fig. 3b), similar with that of BBOA.

The average CCOA mass concentration was 6.4 μg m^{-3}, accounting for 22.0% of total OA mass (Fig. 8a). The mass fraction of CCOA could reach to ~30% of OA during night and decreased to 3% during afternoon (Fig. 8b). This indicates that CCOA was an important OA component similar as that in Beijing OA (15–55%) (Zhang et al., 2014; Elser et al., 2016), but its mass fraction of $PM_{2.5}$ (~9%) was at the low end of the values observed at Beijing and Xi'an (9–21%) (Huang et al., 2014).

3.4.5 LO-OOA and MO-OOA

Two or more OOA components are commonly separated by PMF in urban areas which correspond to fresh SOA and aged SOA (Jimenez et al., 2009), and the MS of SOA factors all have predominant contributions at *m*/*z* 43 and 44. The MS of fresher SOA such as LO-OOA has higher contribution at *m*/*z* 43 (mainly $C_2H_3O^+$, accounting for 74% of *m*/*z* 43 in this study), while aged SOA such as MO-OOA has higher signal at *m*/*z* 44 (mainly CO_2^+, accounting for 99% of *m*/*z* 44 in this study). The contribution of $C_xH_yO_1^+$ in LO-OOA was 36.8% followed by $C_xH_y^+$ (48.0%), $C_xH_yO_2^+$ (10.3%), $H_yO_1^+$ (1.6%), $C_xH_yN_p^+$ (2.8%), and $C_xH_yO_zN_p^+$ (0.5%) (Fig. S9). The O/C ratio of LO-OOA was 0.33 and H/C was 1.47 consistent with fresh SOA. The MS of MO-OOA was comprised of 25.3% of $C_xH_yO_2^+$, 35.7% of $C_xH_yO_1^+$, 30.1% of $C_xH_y^+$, 6.7% of $H_xO_1^+$, 1.8% of $C_xH_yN_p^+$,

and 0.4% of $C_xH_yO_zN_p^+$ (Fig. S9). The O/C and H/C ratios of MO-OOA were 0.80 and 1.14, respectively. These results indicate that the atmospheric oxidation capacity during winter was still somewhat strong. The positions of LO-OOA and MO-OOA in triangle plot of fCO_2^+ *vs*. $fC_2H_3O^+$ are situated in the space of triangle plot with MO-OOA at the upper left corner (Fig. 9b) and LO-OOA at the lower right space, respectively, suggesting the different oxidation degree of OOA factors. The MS of LO-OOA and MO-OOA were similar with those of summer 2012 (R^2 = 0.95 for MO-OOA and R^2 = 0.80 for LO-OOA, Fig. S11). Note that the $C_xH_y^+$ ions in LO-OOA were mainly from by *m*/*z* 39, 41, 91 and 115 (Fig. 7h), which were also found to be enriched in coal combustion organic aerosols. This feature is similar to that of summer 2012, potentially suggesting that part of LO-OOA was from further oxidation of CCOA.

The temporal variations of LO-OOA and MO-OOA were highly correlated with secondary inorganic species: LO-OOA *vs*. sulphate (R^2 = 0.71) and MO-OOA *vs*. nitrate (R^2 = 0.71) (Fig. 7a and b, Table 2). These patterns are somewhat contradictory to previous AMS findings that LO-OOA typically correlates better with nitrate due to their similar semi-volatile characteristics while MO-OOA tends to correlate better with sulphate as they are both low-volatility species. These correlations were indeed observed during the summer study of 2012 (Xu et al., 2014). The behaviours of the two OOA factors during this study were likely due to the low air temperature and low RH conditions which favoured nitrate formation primarily through photochemical reactions. This phenomenon was also observed in winter time of Beijing (Sun et al., 2013b).

The diurnal variation profiles of LO-OOA and MO-OOA all showed one bump with the LO-OOA peaking between 11:00–14:00 and MO-OOA peaking between 12:00–18:00, suggesting the importance of photochemical processes for both OOA factors. The size distribution of the OOA (LO-OOA + MO-OOA) had a mode size of ~550 nm (Fig. 3b) reflecting the feature as SOA. This size mode is slightly bigger than those of OOA in

718 other studies such as Fresno (460 nm) and Lanzhou summer 2012 (~450 nm) likely due
719 to the high concentration of gas precursors and longer lifecycle of aerosol during winter.

720

721 The mass concentrations of LO-OOA and MO-OOA were 6.5 and 4.4 μg m^{-3} with the
722 mass contributions of 22.3% and 14.9% to OA, respectively (Fig. 8a). These
723 contributions were lower than those during summer 2012 in Lanzhou (27% for LO-OOA
724 and 32% for MO-OOA) especially for MO-OOA, likely due to the relative weak solar
725 radiation during winter and more primary sources in winter. The diurnal total
726 contribution of OOA (LO-OOA + MO-OOA) varied between 20%–60% (Fig. 8b),
727 suggesting the importance of SOA in the air pollution throughout the day at Lanzhou.

728

729 3.5 Primary and secondary OA

730 As shown in Fig. 2b, the mass fraction of organics increased with the increase of PM_1
731 concentration, so it is important to know the relative contributions of primary and
732 secondary OA components during the pollution periods. Fig. 10a shows the scatter plot of
733 SOA (= LO-OOA + MO-OOA) and POA (= HOA + BBOA + COA + CCOA) during this
734 study. It is clear that POA and SOA show relative tight correlation during the periods of
735 POA less than ~15 μg m^{-3} associated with low mass fractions of OA. When POA and
736 OA fraction increased significantly, POA and SOA show almost no correlation,
737 indicating the importance of POA in the severe aerosol pollutions in Lanzhou during
738 winter. This is different than the observation from summer 2012, during which SOA had
739 a stable contribution to PM_1 (Fig. 10b), due to more complex POA sources and larger
740 contributions from these sources to PM_1 mass loading during winter compared to
741 summer. This is even more evident when comparing each POA factor with OA (Fig. 11).
742 The COA had the biggest contribution to the increased organics can explained 51% of the
743 increase of organics, followed by CCOA (19%). The components of HOA and BBOA
744 also had positive contributions to the increase of PM_1 mass. However, both OOA
745 components had negative slopes with organics with LO-OOA being the major one. The

746 phenomenon of POA dominating during haze periods is different from the results in other
747 cities in China (Huang et al., 2014). For example, Elser et al. (2016) found significant
748 increased contribution from SOA and secondary inorganic aerosol during haze periods in
749 2013/2014 winter in Xi'an and Beijing. This is likely due to the higher RH values in the
750 eastern China which is more favourable for the aqueous-phase production of SOA.
751 Indeed, Sun et al. (2013a) observed significant increase of secondary inorganic aerosol
752 during high RH periods in Beijing.

753

754 The average contribution of POA to organics decreased from 63.0% to 39.3% during
755 Chinese New Year festival of 2014 (Fig. 1) due to the reduced primary aerosol sources
756 (many restaurants were closed during the holiday of Chinese New Year) such as HOA
757 (9.8% to 3.3%), COA (20.2% to 11.6%), CCOA (22.0% to 15.4%), and BBOA (10.8% to
758 9.0%). This is an indication that control of cooking activities and traffic emissions in this
759 residential area may be effective strategies for air quality improvement during winter.

760

761 3.6 Fossil and non-fossil OC

762 OC measured by OC/EC analyser on two filters (OC_{filter}) and corresponding AMS
763 (OC_{AMS}) online measured results are shown in Fig. 12a. The average ratio of
764 OC_{AMS}/OC_{filter} was ~1.5 for these two filters likely due to the analytical uncertainties of
765 different instruments (30% for AMS and 20% for OC_{filter}), which was also observed in
766 other studies (Zotter et al., 2014). The data from the ^{14}C measurement for the filter
767 samples are listed in Table S1. The total average of f_{NF} in these four filters was 55 ± 3%,
768 with 54% and 57% for filters during Jan. 15 and Jan. 23, respectively. Comparison with
769 other studies, the average f_{NF} value in this study was lower than those in Xi'an (63%) and
770 Guangzhou (65%), and higher than those in Beijing (42%), while similar with those in
771 Shanghai (51%) during 2012/2013 winter (Zhang et al., 2015b). Combining with the f_{NF}
772 value (the total average of f_{NF} for the total average AMS results) and the contributions of
773 fossil (F) POC (HOC and CCOC) and non-fossil (NF) POC (BBOC and COC), the f_F and
774 f_{NF} for SOC could be obtained (Fig. 12b). The average f_F and f_{NF} for POC and SOC are

775 summarized into Fig. 13. The f_F and f_{NF} for POC during Jan. 15 were 50% and 50%,
776 while for SOC were 32% and 68%. The f_F and f_{NF} for POC during Jan. 23 were 37% and
777 63%, while for SOC were 56% and 44%. For all AMS data, the f_F and f_{NF} in POC were
778 50% and 50%, while for SOC were 34% and 66%. The F-POC during Jan. 15 and Jan. 23
779 were comprised by 15% and 16% HOC and 35% and 21% CCOC, respectively, and NF-
780 POC by 18% and 13% BBOC and 32% and 50% COC, respectively. For all AMS data,
781 the F-POC was comprised by 17% HOC and 33% CCOC, and NF-POC by 16% BBOC
782 and 34% COC.

783

784 3.7 Evolution of OA and relationship between odd oxygen and SOA

785 The evolution of OA chemical composition upon aging has been an important subject
786 which is used to understand the formation of SOA. The methods to characterize this
787 evolution include the application of several specific diagrams, such as the AMS triangle
788 plot (*f*44 *vs*. *f*43 or fCO_2^+ *vs*. $fC_2H_3O^+$) (Ng et al., 2010) and Van Krevelent plot (H:C *vs*.
789 O:C) (Heald et al., 2010). In the plot of *f*44 *vs*. *f*43 of this study (Fig. 9a), the data
790 distributed in a narrow space and move up vertically in the triangle space suggesting
791 significant increasing in *f*44. The data from the low (night time) to the high (afternoon
792 time) *f*44 value corresponded to the evolution of the photo radiation intensity suggesting
793 the photochemical processes. In the plot of fCO_2^+ *vs*. $fC_2H_3O^+$ (Fig. 9b), most of data
794 moved out of triangle space because of the high contribution of $C_3H_7^+$ at *m*/*z* 43,
795 especially for data during night time. fCO_2^+ and $fC_2H_3O^+$ both increased before the noon
796 time, after that $fC_2H_3O^+$ stopped at ~0.06 and fCO_2^+ kept increase likely suggesting the
797 evolution of LO-OOA to MO-OOA. In comparison to the results in summer 2012, the
798 data in winter were more concentrated in the triangle space suggesting air masses with
799 similar source contribution during winter. The winter data in the Van Krevelen diagram
800 follows a slope of −0.8 (Fig. 14a) which suggest that SOA formation chemistry was a
801 combination of carboxylic acid and alcohol/peroxide formation (−1 to −0.5). This slope is
802 higher than that observed at Changdao (−0.6, rural site) in China during winter
803 suggesting the less oxidation state of our data.

In order to understand the possible sources of oxygenated OA, we also compared the diurnal variations between MO-OOA and O_x (Fig. 14b). Both O_x and OOA are products of photochemical reactions and the comparison between O_x and OOA can offer insight into the formation of OA due to the dependence of the ratio on the VOC species (Herndon et al., 2008), assuming aqueous processing and night time oxidation for OOA were less important, such as during this study due to the low RH. High SOA *vs*. O_x slopes were observed (larger than 0.12 μg m^{-3} ppb^{-1}) where aromatic VOC dominated the photochemical processing, while a low slopes (~0.03 μg m^{-3} ppb^{-1}) were observed where alkene VOCs dominated the photochemical processing (Wood et al., 2010; Hayes et al., 2013). Fig. 14b shows the scatter plot between O_x and MO-OOA and sized by the mass concentration of BBOA. O_x and MO-OOA showed tight correlation (R^2 = 0.95) with a slope of 0.11 μg m^{-3} ppb^{-1}. This result is similar with that found in Beijing during wintertime, which has suggested that semivolatile VOCs (e.g., PAHs) could be the primary precursor of OOA (Hu et al., 2016). Several studies suggested that aromatic VOC is dominant among VOCs in northern China (Zhang et al., 2015c) and can be important contribution for SOA production (Liu et al. 2012). We also did correlation between LO-OOA and Ox, and found the different synchronization of LO-OOA and Ox (Fig. S12). It seems LO-OOA varied two to three hours earlier than Ox, likely suggesting other origination for LO-OOA such as down mixing of mixing-layer aerosol, which is a popular phenomenon in the mountain-valley city (Chen et al., 2009).

4 Conclusions

In order to understand the sources and chemical processes of the air pollution during winter in Lanzhou, a field study was conducted at an urban site of Lanzhou during January 10 – February 4, 2014 using a suit of on-line instruments. The results show that the average mass concentration of PM_1 (NR-PM_1 + BC) was 57.3 μg m^{-3} (ranging from 2.1 to 229.7 μg m^{-3} for hourly averages), with 51.2% of organics, 16.5% of nitrate, 12.5% of sulphate, 10.3% of ammonium, 6.4% of BC, and 3.0% of chloride. This mass

concentration was about two times higher than that during summer 2012 in Lanzhou, however, the mass loading levels and chemical compositions were similar to those observed in Beijing during winter. The mass concentration of nitrate and organics increased with the increase of PM_1 loading, while sulphate decreased, indicating the importance of OA and nitrate during severe air pollution. The size distributions of all the species displayed a moderate size at 400–500 nm, suggesting that aerosol particles were largely internally mixed during winter. All species presented significant diurnal variations. BC had two peaks at 10:00–12:00 and 20:00–22:00, respectively. Further analysis indicated that the first peak was resulted from the contribution of multiple combustion sources and could be related with the variations of the boundary layer heights during morning which accumulated the air pollutants from early morning and until the break-up at around noon time (such influences should be further verified in the future with simultaneous measurements from boundary layer heights). The evening peak of BC was related to human activities such as traffic and coal combustion coupled with the shallow PBL. OA presented two peaks corresponding to lunch and dinner time suggesting cooking to be an important source. Sulphate peaked during the noon time (11:00–14:00) indicating the importance of photochemical processes. Nitrate presented an afternoon peak (12:00–16:00) which indicate the photochemical processing of NOx. The diurnal pattern of nitrate during winter time was significant different from that during summer 2012 which was thought mainly from the mixing down of aloft residual layer. PMF analysis of organic mass spectrum with the ME-2 engine identified six organic aerosol sources: i.e., HOA, BBOA, COA, CCOA, LO-OOA, and MO-OOA. POA, which includes HOA, BBOA, COA, and CCOA, accounted for 63% of OA mass and showed an increased in concentration with the increase of PM_1 loading. This is an indication that POA emission was one of the main reasons for the occurrence of heavy air pollution episodes. The temporal profile of MO-OOA tightly correlated with that of nitrate, while those of LO-OOA with sulphate correlated. This observation was different than those observed during other studies and during summer at Lanzhou, indicating the importance of photochemistry for nitrate during winter in Lanzhou due to cold air

862 temperature and low RH conditions. ^{14}C analysis of OOC indicated that 66% of the SOC
863 was formed from non-fossil source.

864

865 **Acknowledgements**

866 The authors thank their colleagues for continuing support and discussion. This research
867 was supported by grants from the Chinese Academy of Sciences Hundred Talents
868 Program, the Key Laboratory of Cryospheric Sciences Scientific Research Foundation
869 (SKLCS-ZZ-2015-01), the National Natural Science Foundation of China Science Fund
870 for Creative Research Groups (41121001, 21407079, 91544220), and the Chinese
871 Academy of Sciences Key Research Program (KJZD-EW-G03).

872 **References**

873

874 Abdullahi, K. L., Delgado-Saborit, J. M., and Harrison, R. M.: Emissions and indoor
875 concentrations of particulate matter and its specific chemical components from
876 cooking: A review, Atmos. Environ., 71, 260-294,
877 doi:10.1016/j.atmosenv.2013.01.061,2013.

878 Agrios, K., Salazar, G. A., Zhang, Y. L., Uglietti, C., Battaglia, M., Luginbühl, M.,
879 Ciobanu, V. G., Vonwiller, M., and Szidat, S.: Online coupling of pure O_2
880 thermo-optical methods - ^{14}C AMS for source apportionment of carbonaceous
881 aerosols study, Nucl. Instrum. Meth. Phys. Res. B., 361, 288-293,
882 doi:10.1016/j.nimb.2015.06.008, 2015.

883 Aiken, A. C., DeCarlo, P. F., Kroll, J. H., Worsnop, D. R., Huffman, J. A., Docherty, K.
884 S., Ulbrich, I. M., Mohr, C., Kimmel, J. R., Sueper, D., Sun, Y., Zhang, Q.,
885 Trimborn, A., Northway, M., Ziemann, P. J., Canagaratna, M. R., Onasch, T. B.,
886 Alfarra, M. R., Prevot, A. S. H., Dommen, J., Duplissy, J., Metzger, A.,
887 Baltensperger, U., and Jimenez, J. L.: O/C and OM/OC ratios of primary,
888 secondary, and ambient organic aerosols with high-resolution time-of-flight
889 aerosol mass spectrometry, Environ. Sci. Technol., 42, 4478-4485,
890 doi:10.1021/es703009q, 2008.

891 Alfarra, M. R., Prevot, A. S. H., Szidat, S., Sandradewi, J., Weimer, S., Lanz, V. A.,
892 Schreiber, D., Mohr, M., and Baltensperger, U.: Identification of the Mass
893 Spectral Signature of Organic Aerosols from Wood Burning Emissions, Environ.
894 Sci. Technol., 41, 5770-5777, doi:10.1021/es062289b, 2007.

895 Beekmann, M., Prévôt, A. S. H., Drewnick, F., Sciare, J., Pandis, S. N., Denier van der
896 Gon, H. A. C., Crippa, M., Freutel, F., Poulain, L., Ghersi, V., Rodriguez, E.,
897 Beirle, S., Zotter, P., von der Weiden-Reinmüller, S.-L., Bressi, M., Fountoukis,
898 C., Petetin, H., Szidat, S., Schneider, J., Rosso, A., El Haddad, I., Megaritis, A.,
899 Zhang, Q. J., Michoud, V., Slowik, J. G., Moukhtar, S., Kolmonen, P., Stohl, A.,
900 Eckhardt, S., Borbon, A., Gros, V., Marchand, N., Jaffrezo, J. L.,
901 Schwarzenboeck, A., Colomb, A., Wiedensohler, A., Borrmann, S., Lawrence,
902 M., Baklanov, A., and Baltensperger, U.: In situ, satellite measurement and model
903 evidence on the dominant regional contribution to fine particulate matter levels in
904 the Paris megacity, Atmos. Chem. Phys., 15, 9577-9591, doi:10.5194/acp-15-
905 9577-2015, 2015.

906 Bi, J., Huang, J., Hu, Z., Holben, B. N., and Guo, Z.: Investigating the aerosol optical and
907 radiative characteristics of heavy haze episodes in Beijing during January of 2013,
908 J. Geophys. Res., 119, 9884-9900, doi:10.1002/2014JD021757, 2014.

909 Bond, T., and Bergstrom, R.: Light absorption by carbonaceous particles: An
910 investigative review, Aerosol. Sci. Tech., 40, 27–67,
911 doi:10.1080/02786820500421521, 2006.

912 Canagaratna, M. R., Jayne, J. T., Jimenez, J. L., Allan, J. D., Alfarra, M. R., Zhang, Q.,
913 Onasch, T. B., Drewnick, F., Coe, H., Middlebrook, A., Delia, A., Williams, L.
914 R., Trimborn, A. M., Northway, M. J., DeCarlo, P. F., Kolb, C. E., Davidovits, P.,
915 and Worsnop, D. R.: Chemical and microphysical characterization of ambient
916 aerosols with the aerodyne aerosol mass spectrometer, Mass Spectrom. Rev., 26,
917 185-222, doi:10.1002/mas.20115, 2007.

918 Canagaratna, M. R., Jimenez, J. L., Kroll, J. H., Chen, Q., Kessler, S. H., Massoli, P.,
919 Hildebrandt Ruiz, L., Fortner, E., Williams, L. R., Wilson, K. R., Surratt, J. D.,
920 Donahue, N. M., Jayne, J. T., and Worsnop, D. R.: Elemental ratio measurements
921 of organic compounds using aerosol mass spectrometry: Characterization,
922 improved calibration, and implications, Atmos. Chem. Phys., 15, 253-272,
923 doi:10.5194/acp-15-253-2015, 2015.

924 Canonaco, F., Crippa, M., Slowik, J. G., Baltensperger, U., and Prévôt, A. S. H.: SoFi, an
925 IGOR-based interface for the efficient use of the generalized multilinear engine
926 (ME-2) for the source apportionment: ME-2 application to aerosol mass
927 spectrometer data, Atmos. Meas. Tech., 6, 3649-3661, doi:10.5194/amt-6-3649-
928 2013, 2013.

929 Cao, C., Jiang, W., Wang, B., Fang, J., Lang, J., Tian, G., Jiang, J., and Zhu, T. F.:
930 Inhalable Microorganisms in Beijing's PM2.5 and PM10 Pollutants during a
931 Severe Smog Event, Environ. Sci. Technol., 48, 1499-1507,
932 doi:10.1021/es4048472, 2014.

933 Carlton, A. G., Bhave, P. V., Napelenok, S. L., Edney, E. O., Sarwar, G., Pinder, R. W.,
934 Pouliot, G. A., and Houyoux, M.: Model Representation of Secondary Organic
935 Aerosol in Cmaqv4.7, Environ. Sci. Technol., 44, 8553-8560,
936 doi:10.1021/es100636q, 2010.

937 Chan, C. K., and Yao, X.: Air pollution in mega cities in China, Atmos. Environ., 42, 1-
938 42, doi:10.1016/j.atmosenv.2007.09.003, 2008.

939 Chen, Y., Zhao, C., Zhang, Q., Deng, Z., Huang, M., and Ma, X.: Aircraft study of
940 Mountain Chimney Effect of Beijing, China, J. Geophys. Res., 114, D08306,
941 10.1029/2008JD010610, 2009.

942 Crippa, M., Canonaco, F., Lanz, V. A., Äijälä, M., Allan, J. D., Carbone, S., Capes, G.,
943 Ceburnis, D., Dall'Osto, M., Day, D. A., DeCarlo, P. F., Ehn, M., Eriksson, A.,
944 Freney, E., Hildebrandt Ruiz, L., Hillamo, R., Jimenez, J. L., Junninen, H.,
945 Kiendler-Scharr, A., Kortelainen, A. M., Kulmala, M., Laaksonen, A., Mensah,
946 A. A., Mohr, C., Nemitz, E., O'Dowd, C., Ovadnevaite, J., Pandis, S. N., Petäjä,
947 T., Poulain, L., Saarikoski, S., Sellegri, K., Swietlicki, E., Tiitta, P., Worsnop, D.
948 R., Baltensperger, U., and Prévôt, A. S. H.: Organic aerosol components derived
949 from 25 AMS data sets across Europe using a consistent ME-2 based source
950 apportionment approach, Atmos. Chem. Phys., 14, 6159-6176, doi:10.5194/acp-
951 14-6159-2014, 2014.

952 Crippa, M., DeCarlo, P. F., Slowik, J. G., Mohr, C., Heringa, M. F., Chirico, R., Poulain,
953 L., Freutel, F., Sciare, J., Cozic, J., Di Marco, C. F., Elsasser, M., Nicolas, J. B.,

Marchand, N., Abidi, E., Wiedensohler, A., Drewnick, F., Schneider, J., Borrmann, S., Nemitz, E., Zimmermann, R., Jaffrezo, J. L., Prévôt, A. S. H., and Baltensperger, U.: Wintertime aerosol chemical composition and source apportionment of the organic fraction in the metropolitan area of paris, Atmos. Chem. Phys., 13, 961-981, doi:10.5194/acp-13-961-2013, 2013.

Dall'Osto, M., Ovadnevaite, J., Ceburnis, D., Martin, D., Healy, R. M., O'Connor, I. P., Kourtchev, I., Sodeau, J. R., Wenger, J. C., and O'Dowd, C.: Characterization of urban aerosol in Cork city (Ireland) using aerosol mass spectrometry, Atmos. Chem. Phys., 13, 4997-5015, doi:10.5194/acp-13-4997-2013, 2013.

DeCarlo, P. F., Kimmel, J. R., Trimborn, A., Northway, M. J., Jayne, J. T., Aiken, A. C., Gonin, M., Fuhrer, K., Horvath, T., Docherty, K. S., Worsnop, D. R., and Jimenez, J. L.: Field-Deployable, High-Resolution, Time-of-Flight Aerosol Mass Spectrometer, Anal. Chem., 78, 8281-8289, doi:10.1021/ac061249n, 2006.

Du, W., Sun, Y. L., Xu, Y. S., Jiang, Q., Wang, Q. Q., Yang, W., Wang, F., Bai, Z. P., Zhao, X. D., and Yang, Y. C.: Chemical characterization of submicron aerosol and particle growth events at a national background site (3295 m a.s.l.) on the Tibetan Plateau, Atmos. Chem. Phys., 15, 10811-10824, doi:10.5194/acp-15-10811-2015, 2015.

Elser, M., Huang, R. J., Wolf, R., Slowik, J. G., Wang, Q., Canonaco, F., Li, G., Bozzetti, C., Daellenbach, K. R., Huang, Y., Zhang, R., Li, Z., Cao, J., Baltensperger, U., El-Haddad, I., and Prévôt, A. S. H.: New insights into pm2.5 chemical composition and sources in two major cities in china during extreme haze events using aerosol mass spectrometry, Atmos. Chem. Phys., 16, 3207-3225, doi:10.5194/acp-16-3207-2016, 2016.

Ge, X., Setyan, A., Sun, Y., and Zhang, Q.: Primary and secondary organic aerosols in Fresno, California during wintertime: Results from high resolution aerosol mass spectrometry, J. Geophys. Res., 117, D19301, doi:10.1029/2012jd018026, 2012.

Hayes, P. L., Ortega, A. M., Cubison, M. J., Froyd, K. D., Zhao, Y., Cliff, S. S., Hu, W. W., Toohey, D. W., Flynn, J. H., Lefer, B. L., Grossberg, N., Alvarez, S., Rappenglück, B., Taylor, J. W., Allan, J. D., Holloway, J. S., Gilman, J. B., Kuster, W. C., de Gouw, J. A., Massoli, P., Zhang, X., Liu, J., Weber, R. J., Corrigan, A. L., Russell, L. M., Isaacman, G., Worton, D. R., Kreisberg, N. M., Goldstein, A. H., Thalman, R., Waxman, E. M., Volkamer, R., Lin, Y. H., Surratt, J. D., Kleindienst, T. E., Offenberg, J. H., Dusanter, S., Griffith, S., Stevens, P. S., Brioude, J., Angevine, W. M., and Jimenez, J. L.: Organic aerosol composition and sources in Pasadena, California during the 2010 CalNex campaign, J. Geophys. Res., 118, 9233-9257, doi:10.1002/jgrd.50530, 2013.

He, K., Yang, F., Ma, Y., Zhang, Q., Yao, X., Chan, C. K., Cadle, S., Chan, T., and Mulawa, P.: The characteristics of PM2.5 in Beijing, China, Atmos. Environ., 35, 4959-4970, doi:10.1016/s1352-2310(01)00301-6, 2001.

He, L.-Y., Huang, X.-F., Xue, L., Hu, M., Lin, Y., Zheng, J., Zhang, R., and Zhang, Y.-H.: Submicron aerosol analysis and organic source apportionment in an urban

atmosphere in Pearl River Delta of China using high-resolution aerosol mass spectrometry, J. Geophys. Res., 116, D12304, doi:10.1029/2010jd014566, 2011.

He, L. Y., Lin, Y., Huang, X. F., Guo, S., Xue, L., Su, Q., Hu, M., Luan, S. J., and Zhang, Y. H.: Characterization of high-resolution aerosol mass spectra of primary organic aerosol emissions from Chinese cooking and biomass burning, Atmos. Chem. Phys., 10, 11535-11543, doi:10.5194/acp-10-11535-2010, 2010.

Heald, C. L., Kroll, J. H., Jimenez, J. L., Docherty, K. S., DeCarlo, P. F., Aiken, A. C., Chen, Q., Martin, S. T., Farmer, D. K., and Artaxo, P.: A Simplified Description of the Evolution of Organic Aerosol Composition in the Atmosphere, Geophys. Res. Lett., 37, L08803, doi:10.1029/2010gl042737, 2010.

Herndon, S. C., Onasch, T. B., Wood, E. C., Kroll, J. H., Canagaratna, M. R., Jayne, J. T., Zavala, M. A., Knighton, W. B., Mazzoleni, C., Dubey, M. K., Ulbrich, I. M., Jimenez, J. L., Seila, R., de Gouw, J. A., de Foy, B., Fast, J., Molina, L. T., Kolb, C. E., and Worsnop, D. R.: Correlation of secondary organic aerosol with odd oxygen in Mexico City, Geophys. Res. Lett., 35, L15804, doi:10.1029/2008GL034058, 2008.

Hodzic, A., Kasibhatla, P. S., Jo, D. S., Cappa, C. D., Jimenez, J. L., Madronich, S., and Park, R. J.: Rethinking the Global Secondary Organic Aerosol (Soa) Budget: Stronger Production, Faster Removal, Shorter Lifetime, Atmos. Chem. Phys., 16, 7917-7941, doi:10.5194/acp-16-7917-2016, 2016.

Hu, W. W., Hu, M., Yuan, B., Jimenez, J. L., Tang, Q., Peng, J. F., Hu, W., Shao, M., Wang, M., Zeng, L. M., Wu, Y. S., Gong, Z. H., Huang, X. F., and He, L. Y.: Insights on organic aerosol aging and the influence of coal combustion at a regional receptor site of central eastern China, Atmos. Chem. Phys., 13, 10095-10112, doi:10.5194/acp-13-10095-2013, 2013.

Hu, W., Hu, M., Hu, W., Jimenez, J. L., Yuan, B., Chen, W., Wang, M., Wu, Y., Chen, C., Wang, Z., Peng, J., Zeng, L., and Shao, M.: Chemical Composition, Sources, and Aging Process of Submicron Aerosols in Beijing: Contrast between Summer and Winter, J. Geophys. Res., 121, 2015JD024020, doi: 10.1002/2015JD024020, 2016.

Huang, R.-J., Zhang, Y., Bozzetti, C., Ho, K.-F., Cao, J.-J., Han, Y., Daellenbach, K. R., Slowik, J. G., Platt, S. M., Canonaco, F., Zotter, P., Wolf, R., Pieber, S. M., Bruns, E. A., Crippa, M., Ciarelli, G., Piazzalunga, A., Schwikowski, M., Abbaszade, G., Schnelle-Kreis, J., Zimmermann, R., An, Z., Szidat, S., Baltensperger, U., Haddad, I. E., and Prevot, A. S. H.: High secondary aerosol contribution to particulate pollution during haze events in China, Nature, 514, 218-222, doi:10.1038/nature13774, 2014

Huang, X.-F., Xue, L., Tian, X.-D., Shao, W.-W., Sun, T.-L., Gong, Z.-H., Ju, W.-W., Jiang, B., Hu, M., and He, L.-Y.: Highly time-resolved carbonaceous aerosol characterization in Yangtze River Delta of China: Composition, mixing state and secondary formation, Atmos. Environ., 64, 200-207, doi:10.1016/j.atmosenv.2012.09.059, 2013.

1038 Huang, X. F., He, L. Y., Hu, M., Canagaratna, M. R., Kroll, J. H., Ng, N. L., Zhang, Y.
1039 H., Lin, Y., Xue, L., Sun, T. L., Liu, X. G., Shao, M., Jayne, J. T., and Worsnop,
1040 D. R.: Characterization of submicron aerosols at a rural site in Pearl River Delta
1041 of China using an Aerodyne High-Resolution Aerosol Mass Spectrometer, Atmos.
1042 Chem. Phys., 11, 1865-1877, doi:10.5194/acp-11-1865-2011, 2011.

1043 Ianniello, A., Spataro, F., Esposito, G., Allegrini, I., Hu, M., and Zhu, T.: Chemical
1044 characteristics of inorganic ammonium salts in PM2.5 in the atmosphere of
1045 Beijing (China), Atmos. Chem. Phys., 11, 10803-10822, doi:10.5194/acp-11-
1046 10803-2011, 2011.

1047 Jayne, J. T., Leard, D. C., Zhang, X., Davidovits, P., Smith, K. A., Kolb, C. E., and
1048 Worsnop, D. R.: Development of an Aerosol Mass Spectrometer for Size and
1049 Composition Analysis of Submicron Particles, Aerosol. Sci. Tech., 33, 49 - 70,
1050 doi:10.1080/027868200410840, 2000.

1051 Jimenez, J. L., Canagaratna, M. R., Donahue, N. M., Prevot, A. S. H., Zhang, Q., Kroll, J.
1052 H., DeCarlo, P. F., Allan, J. D., Coe, H., Ng, N. L., Aiken, A. C., Docherty, K. S.,
1053 Ulbrich, I. M., Grieshop, A. P., Robinson, A. L., Duplissy, J., Smith, J. D.,
1054 Wilson, K. R., Lanz, V. A., Hueglin, C., Sun, Y. L., Tian, J., Laaksonen, A.,
1055 Raatikainen, T., Rautiainen, J., Vaattovaara, P., Ehn, M., Kulmala, M.,
1056 Tomlinson, J. M., Collins, D. R., Cubison, M. J., E., Dunlea, J., Huffman, J. A.,
1057 Onasch, T. B., Alfarra, M. R., Williams, P. I., Bower, K., Kondo, Y., Schneider,
1058 J., Drewnick, F., Borrmann, S., Weimer, S., Demerjian, K., Salcedo, D., Cottrell,
1059 L., Griffin, R., Takami, A., Miyoshi, T., Hatakeyama, S., Shimono, A., Sun, J. Y.,
1060 Zhang, Y. M., Dzepina, K., Kimmel, J. R., Sueper, D., Jayne, J. T., Herndon, S.
1061 C., Trimborn, A. M., Williams, L. R., Wood, E. C., Middlebrook, A. M., Kolb, C.
1062 E., Baltensperger, U., and Worsnop, D. R.: Evolution of organic aerosols in the
1063 atmosphere, Science, 326, 1525-1529, doi:10.1126/science.1180353, 2009.

1064 Liu, Z., Wang, Y., Vrekoussis, M., Richter, A., Wittrock, F., Burrows, J. P., Shao, M.,
1065 Chang, C.-C., Liu, S.-C., Wang, H., and Chen, C.: Exploring the missing source
1066 of glyoxal (CHOCHO) over China, Geophys. Res. Lett., 39, L10812,
1067 doi:10.1029/2012GL051645, 2012.

1068 Minguillón, M. C., Perron, N., Querol, X., Szidat, S., Fahrni, S. M., Alastuey, A.,
1069 Jimenez, J. L., Mohr, C., Ortega, A. M., Day, D. A., Lanz, V. A., Wacker, L.,
1070 Reche, C., Cusack, M., Amato, F., Kiss, G., Hoffer, A., Decesari, S., Moretti, F.,
1071 Hillamo, R., Teinilä, K., Seco, R., Peñuelas, J., Metzger, A., Schallhart, S.,
1072 Müller, M., Hansel, A., Burkhart, J. F., Baltensperger, U., and Prévôt, A. S. H.:
1073 Fossil versus contemporary sources of fine elemental and organic carbonaceous
1074 particulate matter during the DAURE campaign in Northeast Spain, Atmos.
1075 Chem. Phys., 11, 12067-12084, doi:10.5194/acp-11-12067-2011, 2011.

1076 Mohr, C., DeCarlo, P. F., Heringa, M. F., Chirico, R., Slowik, J. G., Richter, R., Reche,
1077 C., Alastuey, A., Querol, X., Seco, R., Penuelas, J., Jimenez, J. L., Crippa, M.,
1078 Zimmermann, R., Baltensperger, U., and Prevot, A. S. H.: Identification and
1079 quantification of organic aerosol from cooking and other sources in Barcelona

using aerosol mass spectrometer data, Atmos. Chem. Phys., 12, 1649-1665, doi:10.5194/acp-12-1649-2012, 2012.

Ng, N. L., Canagaratna, M. R., Zhang, Q., Jimenez, J. L., Tian, J., Ulbrich, I. M., Kroll, J. H., Docherty, K. S., Chhabra, P. S., Bahreini, R., Murphy, S. M., Seinfeld, J. H., Hildebrandt, L., Donahue, N. M., DeCarlo, P. F., Lanz, V. A., Prévôt, A. S. H., Dinar, E., Rudich, Y., and Worsnop, D. R.: Organic aerosol components observed in Northern Hemispheric datasets from Aerosol Mass Spectrometry, Atmos. Chem. Phys., 10, 4625-4641, doi:10.5194/acp-10-4625-2010, 2010.

Okuda, T., Naoi, D., Tenmoku, M., Tanaka, S., He, K., Ma, Y., Yang, F., Lei, Y., Jia, Y., and Zhang, D.: Polycyclic Aromatic Hydrocarbons (Pahs) in the Aerosol in Beijing, China, Measured by Aminopropylsilane Chemically-Bonded Stationary-Phase Column Chromatography and Hplc/Fluorescence Detection, Chemosphere, 65, 427-435, doi:10.1016/j.chemosphere.2006.01.064, 2006.

Ortega, A. M., Day, D. A., Cubison, M. J., Brune, W. H., Bon, D., de Gouw, J. A., and Jemenez, J. L., Secondary organic aerosol formation and primary organic aerosol oxidation from biomass-burning smoke in a flow reactor during FLAME-3, Atmos. Chem. Phys., 13(22), 11551-11571, doi:10.5194/acp-13-11551-2013, 2013.

Paatero, P., and Tapper, U.: Positive matrix factorization: A non-negative factor model with optimal utilization of error estimates of data values, Environmetrics, 5, doi:111-126, 10.1002/env.3170050203, 1994.

Pusede, S. E., VandenBoer, T. C., Murphy, J. G., Markovic, M. Z., Young, C. J., Veres, P. R., Roberts, J. M., Washenfelder, R. A., Brown, S. S., Ren, X., Tsai, C., Stutz, J., Brune, W. H., Browne, E. C., Wooldridge, P. J., Graham, A. R., Weber, R., Goldstein, A. H., Dusanter, S., Griffith, S. M., Stevens, P. S., Lefer, B. L., and Cohen, R. C.: An Atmospheric Constraint on the No2 Dependence of Daytime near-Surface Nitrous Acid (Hono), Environ. Sci.Technol., 49, 12774-12781, doi:10.1021/acs.est.5b02511, 2015.

Song, Y., Xie, S., Zhang, Y., Zeng, L., Salmon, L. G., and Zheng, M.: Source apportionment of PM2.5 in Beijing using principal component analysis/absolute principal component scores and UNMIX, Sci. Total. Environ., 372, 278-286, doi:10.1016/j.scitotenv.2006.08.041, 2006.

Sun, Y., Du, W., Fu, P., Wang, Q., Li, J., Ge, X., Zhang, Q., Zhu, C., Ren, L., Xu, W., Zhao, J., Han, T., Worsnop, D. R., and Wang, Z.: Primary and secondary aerosols in Beijing in winter: sources, variations and processes, Atmos. Chem. Phys., 16, 8309-8329, doi:10.5194/acp-16-8309-2016, 2016.

Sun, Y., Jiang, Q., Wang, Z., Fu, P., Li, J., Yang, T., and Yin, Y.: Investigation of the sources and evolution processes of severe haze pollution in Beijing in January 2013, J. Geophys. Res., 119, 2014JD021641, doi:10.1002/2014JD021641, 2014.

1119 Sun, Y., Zhuang, G., Tang, A., Wang, Y., and An, Z.: Chemical Characteristics of PM2.5
1120 and PM10 in Haze−Fog Episodes in Beijing, Environ. Sci. Technol., 40, 3148-
1121 3155, doi:10.1021/es051533g, 2006.

1122 Sun, Y., Zhang, Q., Zheng, M., Ding, X., Edgerton, E. S., and Wang, X.: Characterization
1123 and source apportionment of water-soluble organic matter in atmospheric fine
1124 particles ($pm_{2.5}$) with high-resolution aerosol mass spectrometry and gc-ms,
1125 Environ. Sci. and Technol., 45, 4854 - 4861, doi:10.1021/es200162h, 2011a.

1126 Sun, Y., Zhang, Q., Schwab, J. J., Demerjian, K. L., Chen, W. N., Bae, M. S., Hung, H.
1127 M., Hogrefe, O., Frank, B., Rattigan, O. V., and Lin, Y. C.: Characterization of
1128 the sources and processes of organic and inorganic aerosols in New York city
1129 with a high-resolution time-of-flight aerosol mass apectrometer, Atmos. Chem.
1130 Phys., 11, 1581-1602, doi:10.5194/acp-11-1581-2011, 2011b.

1131 Sun, Y. L., Wang, Z., Fu, P., Jiang, Q., Yang, T., Li, J., and Ge, X.: The impact of
1132 relative humidity on aerosol composition and evolution processes during
1133 wintertime in Beijing, China, Atmos. Environ., 77, 927-934,
1134 doi:10.1016/j.atmosenv.2013.06.019, 2013a.

1135 Sun, Y. L., Wang, Z. F., Fu, P. Q., Yang, T., Jiang, Q., Dong, H. B., Li, J., and Jia, J. J.:
1136 Aerosol composition, sources and processes during wintertime in Beijing, China,
1137 Atmos. Chem. Phys., 13, 4577-4592, doi:10.5194/acp-13-4577-2013, 2013b.

1138 Szidat, S.; Salazar, G. A.; Vogel, E.; Battaglia, M.; Wacker, L.; Synal, H. A.; Türler, A.:
1139 ^{14}C analysis and sample preparation at the new Bern Laboratory for the Analysis
1140 of Radiocarbon with AMS (LARA). Radiocarbon, 56, 561-566,
1141 doi:10.2458/56.17457, 2014.

1142 Tang, X. Y., Tian, B. S., Chen, C. H., and Ren, Z. H.: A study of photochemical smog
1143 pollution and its control stratiges at Xi-Gu district of Lanzhou city, China
1144 Environ. Sci., 5(2), 1-11, 1985. (in Chinese with abstract in Eglish)

1145 Ulbrich, I. M., Canagaratna, M. R., Zhang, Q., Worsnop, D. R., and Jimenez, J. L.:
1146 Interpretation of organic components from Positive Matrix Factorization of
1147 aerosol mass spectrometric data, Atmos. Chem. Phys., 9, 2891-2918,
1148 doi:10.5194/acp-9-2891-2009, 2009.

1149 Volkamer, R., Jimenez, J. L., San Martini, F., Dzepina, K., Zhang, Q., Salcedo, D.,
1150 Molina, L. T., Worsnop, D. R., and Molina, M. J.: Secondary organic aerosol
1151 formation from anthropogenic air pollution: Rapid and higher than expected,
1152 Geophys. Res. Lett., 33, L17811, doi:10.1029/2006GL026899, 2006.

1153 Wang, X., Cotter, E., Iyer, K. N., Fang, J., Williams, B. J., and Biswas, P.: Relationship
1154 between pyrolysis products and organic aerosols formed during coal combustion,
1155 P. Combust. Inst., 35, 2347-2354, doi:10.1016/j.proci.2014.07.073, 2015.

1156 Wang, Y., Ying, Q., Hu, J., and Zhang, H.: Spatial and temporal variations of six criteria
1157 air pollutants in 31 provincial capital cities in China during 2013–2014, Environ.
1158 Int., 73, 413-422, doi:10.1016/j.envint.2014.08.016, 2014.

1159 Wiedensohler, A., Birmili, W., Nowak, A., Sonntag, A., Weinhold, K., Merkel, M.,
1160 Wehner, B., Tuch, T., Pfeifer, S., Fiebig, M., Fjäraa, A. M., Asmi, E., Sellegri, K.,
1161 Depuy, R., Venzac, H., Villani, P., Laj, P., Aalto, P., Ogren, J. A., Swietlicki, E.,
1162 Williams, P., Roldin, P., Quincey, P., Hüglin, C., Fierz-Schmidhauser, R., Gysel,
1163 M., Weingartner, E., Riccobono, F., Santos, S., Grüning, C., Faloon, K.,
1164 Beddows, D., Harrison, R., Monahan, C., Jennings, S. G., O'Dowd, C. D.,
1165 Marinoni, A., Horn, H. G., Keck, L., Jiang, J., Scheckman, J., McMurry, P. H.,
1166 Deng, Z., Zhao, C. S., Moerman, M., Henzing, B., de Leeuw, G., Löschau, G.,
1167 and Bastian, S.: Mobility particle size spectrometers: harmonization of technical
1168 standards and data structure to facilitate high quality long-term observations of
1169 atmospheric particle number size distributions, Atmos. Meas. Tech., 5, 657-685,
1170 doi:10.5194/amt-5-657-2012, 2012.

1171 Wood, E. C., Canagaratna, M. R., Herndon, S. C., Onasch, T. B., Kolb, C. E., Worsnop,
1172 D. R., Kroll, J. H., Knighton, W. B., Seila, R., Zavala, M., Molina, L. T.,
1173 DeCarlo, P. F., Jimenez, J. L., Weinheimer, A. J., Knapp, D. J., Jobson, B. T.,
1174 Stutz, J., Kuster, W. C., and Williams, E. J.: Investigation of the correlation
1175 between odd oxygen and secondary organic aerosol in Mexico City and Houston,
1176 Atmos. Chem. Phys., 10, 8947-8968, doi:10.5194/acp-10-8947-2010, 2010.

1177 Xu, J., Zhang, Q., Chen, M., Ge, X., Ren, J., and Qin, D.: Chemical composition, sources,
1178 and processes of urban aerosols during summertime in northwest China: insights
1179 from high-resolution aerosol mass spectrometry, Atmos. Chem. Phys., 14, 12593-
1180 12611, doi:10.5194/acp-14-12593-2014, 2014.

1181 Young, C. J., Washenfelder, R. A., Roberts, J. M., Mielke, L. H., Osthoff, H. D., Tsai,
1182 C., Pikelnaya, O., Stutz, J., Veres, P. R., Cochran, A. K., VandenBoer, T.
1183 C., Flynn, J., Grossberg, N., Haman, C. L., Lefer, B., Stark, H., Graus, M.,
1184 de Grouw, J., Gilman, J. B., Kuster, W. C., and Brown, S. S.: Vertically
1185 resolved measurements of nighttime radical reservoirs in Los Angeles and their
1186 contribution to the urban radical budget, Environ. Sci. Technol., 46, 10965–
1187 10973, doi:10.1021/es302206a, 2012.

1188 Young, D. E., Kim, H., Parworth, C., Zhou, S., Zhang, X., Cappa, C. D., Seco, R., Kim,
1189 S., and Zhang, Q.: Influences of emission sources and meteorology on aerosol
1190 chemistry in a polluted urban environment: results from DISCOVER-AQ
1191 California, Atmos. Chem. Phys., 16, 5427-5451, 10.5194/acp-16-5427-2016,
1192 2016.

1193 Yu, L., Wang, G., Zhang, R., Zhang, L., Song, Y., Wu, B., Li, X., An, K., and Chu, J.:
1194 Characterization and Source Apportionment of PM2.5 in an Urban Environment
1195 in Beijing, Aerosol Air Qual. Res., 13, 574-583, doi:10.4209/aaqr.2012.07.0192,
1196 2013.

1197 Zhang, J. K., Sun, Y., Liu, Z. R., Ji, D. S., Hu, B., Liu, Q., and Wang, Y. S.:
1198 Characterization of submicron aerosols during a month of serious pollution in
1199 Beijing, 2013, Atmos. Chem. Phys., 14, 2887-2903, doi:10.5194/acp-14-2887-
1200 2014, 2014.

1201 Zhang, L., Chen, C., Li, S., and Zhang, F.: Air pollution and potential control schemes in
1202 Lanzhou, Res. Environ. Sci., 13(4), 18-21, 2000.

1203 Zhang, Q., Canagaratna, M. R., Jayne, J. T., Worsnop, D. R., and Jimenez, J. L.: Time-
1204 and size-resolved chemical composition of submicron particles in Pittsburgh:
1205 Implications for aerosol sources and processes, J. Geophys. Res., 110, D07s09,
1206 doi:10.1029/2004jd004649, 2005.

1207 Zhang, Q., Jimenez, J. L., Canagaratna, M. R., Ulbrich, I. M., Ng, N. L., Worsnop, D. R.,
1208 and Sun, Y.: Understanding atmospheric organic aerosols via factor analysis of
1209 aerosol mass spectrometry: a review, Anal. Bioanal. Chem., 401, 3045-3067,
1210 doi:10.1007/s00216-011-5355-y, 2011a.

1211 Zhang, Q., and Li, H.: A studay of the relationship between air pollutants and inversion in
1212 the ABL over the city of Lanzhou, Adv. Atmos. Sci., 28(4), 879-886, doi:
1213 10.1007/s00376-010-0079-z, 2011b.

1214 Zhang, R., Jing, J., Tao, J., Hsu, S. C., Wang, G., Cao, J., Lee, C. S. L., Zhu, L., Chen, Z.,
1215 Zhao, Y., and Shen, Z.: Chemical characterization and source apportionment of
1216 PM2.5 in Beijing: seasonal perspective, Atmos. Chem. Phys., 13, 7053-7074,
1217 doi:10.5194/acp-13-7053-2013, 2013.

1218 Zhang, Y., Schauer, J. J., Zhang, Y., Zeng, L., Wei, Y., Liu, Y., and Shao, M.:
1219 Characteristics of Particulate Carbon Emissions from Real-World Chinese Coal
1220 Combustion, Environ. Sci. Technol., 42, 5068-5073, doi:10.1021/es7022576,
1221 2008.

1222 Zhang, Y. J., Tang, L. L., Wang, Z., Yu, H. X., Sun, Y. L., Liu, D., Qin, W., Canonaco,
1223 F., Prévôt, A. S. H., Zhang, H. L., and Zhou, H. C.: Insights into characteristics,
1224 sources, and evolution of submicron aerosols during harvest seasons in the
1225 Yangtze River delta region, China, Atmos. Chem. Phys., 15, 1331-1349,
1226 doi:10.5194/acp-15-1331-2015, 2015a.

1227 Zhang, Y. L., Huang, R. J., El Haddad, I., Ho, K. F., Cao, J. J., Han, Y., Zotter, P.,
1228 Bozzetti, C., Daellenbach, K. R., Canonaco, F., Slowik, J. G., Salazar, G.,
1229 Schwikowski, M., Schnelle-Kreis, J., Abbaszade, G., Zimmermann, R.,
1230 Baltensperger, U., Prévôt, A. S. H., and Szidat, S.: Fossil vs. Non-fossil sources of
1231 fine carbonaceous aerosols in four chinese cities during the extreme winter haze
1232 episode of 2013, Atmos. Chem. Phys., 15, 1299-1312, 10.5194/acp-15-1299-
1233 2015, 2015b.

1234 Zhang, Y. L.; Perron, N.; Ciobanu, V. G.; Zotter, P.; Minguillón, M. C.; Wacker, L.;
1235 Prévôt, A. S. H.; Baltensperger, U.; Szidat, S.: On the isolation of OC and EC and
1236 the optimal strategy of radiocarbon-based source apportionment of carbonaceous
1237 aerosols. Atmos. Chem. Phys., 12, 10841-10856, doi:10.5194/acp-12-10841-
1238 2012, 2012.

1239 Zhang, Z., Wang, X., Zhang, Y., Lü, S., Huang, Z., Huang, X., and Wang, Y.: Ambient
1240 air benzene at background sites in China's most developed coastal regions:

Exposure levels, source implications and health risks, Sci. Total. Environ., 511, 792-800, doi:10.1016/j.scitotenv.2015.01.003, 2015c.

Zhao, X. J., Zhao, P. S., Xu, J., Meng, W., Pu, W. W., Dong, F., He, D., and Shi, Q. F.: Analysis of a winter regional haze event and its formation mechanism in the North China Plain, Atmos. Chem. Phys., 13, 5685-5696, doi:10.5194/acp-13-5685-2013, 2013.

Zheng, G. J., Duan, F. K., Su, H., Ma, Y. L., Cheng, Y., Zheng, B., Zhang, Q., Huang, T., Kimot, T., Chang, D., Poschl, U., Cheng, Y. F., and He, K. B.: Exploring the severe winter haze in Beijing: the impact of synoptic weather, regional transport and heterogeneous reactions. Atmos. Chem. Phys., **15**(6), 2969-2983 doi:10.5194/acp-15-2969-2015, 2015.

Zheng, M., Salmon, L. G., Schauer, J. J., Zeng, L., Kiang, C. S., Zhang, Y., and Cass, G. R.: Seasonal trends in PM2.5 source contributions in Beijing, China, Atmos. Environ., 39, 3967-3976, doi:10.1016/j.atmosenv.2005.03.036, 2005.

Zotter, P., El-Haddad, I., Zhang, Y., Hayes, P. L., Zhang, X., Lin, Y.-H., Wacker, L., Schnelle-Kreis, J., Abbaszade, G., Zimmermann, R., Surratt, J. D., Weber, R., Jimenez, J. L., Szidat, S., Baltensperger, U., and Prévôt, A. S. H.: Diurnal cycle of fossil and nonfossil carbon using radiocarbon analyses during CalNex, Journal of Geophysical Research: Atmospheres, 119, 6818-6835, doi:10.1002/2013JD021114, 2014.

Table 1 Comparison of the composition of category ions and elemental composition of OA between winter 2013/2014 and summer 2012.

Category Ions	Winter 2014	Summer 2012
$C_xH_y^+$	59%	56%
$C_xH_yO_1^+$	26%	27%
$C_xH_yO_2^+$	10%	11%
$C_xH_yN_p^+$	2%	3%
$C_xH_yN_pO_z^+$	0	1%
$H_yO_1^+$	2%	2%
Elemental composition		
C	67%	59%
H	9%	7%
O	23%	26%
N	1%	1%

Table 2 Coefficient of determination (R^2) between time series of OA factors and other aerosol species.

R^2	HOA	BBOA	COA	CCOA	LO-OOA	MO-OOA	POA*	SOA*
BC	**0.64**	**0.67**	0.24	0.59	0.20	0.06	**0.64**	0.16
PAH	0.40	**0.64**	0.25	0.58	0.02	0.00	**0.61**	0.01
Sulphate	0.35	0.24	0.17	0.22	**0.71**	0.34	0.32	**0.64**
Nitrate	0.19	0.04	0.15	0.02	**0.74**	**0.71**	0.16	**0.85**
Chloride	0.52	0.52	0.19	0.49	0.45	0.13	0.50	0.35
Sulphate + Nitrate	0.27	0.10	0.18	0.07	**0.81**	**0.62**	0.23	**0.85**
Sulphate + Nitrate + Chloride	0.35	0.18	0.19	0.15	**0.77**	0.52	0.32	**0.77**

* POA = HOA + BBOA + COA + CCOA, SOA = LO-OOA + MO-OOA

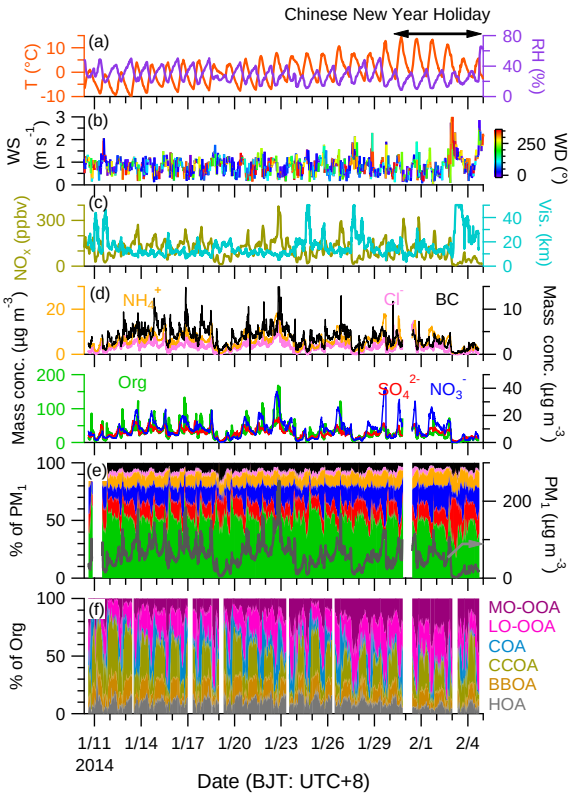

Fig. 1 Summary of meteorological and aerosol species data. (a) air temperature (T) and relative humidity (RH), (b) wind speed (WS) colored by wind direction (WD), (c) NOx and visibility, (d) mass concentration of PM_1 species, (e) the mass contribution of PM1 species (BC is from aethalometer measurement), and (f) the mass contribution of organic components to organic aerosol. Note that BC is from aethalometer measurement.

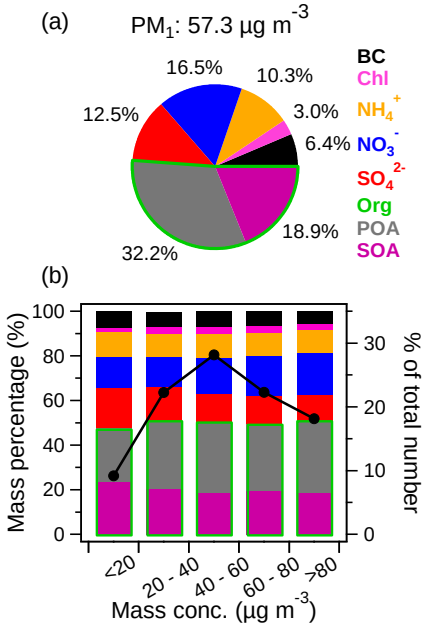

Fig. 2 The average mass contribution of PM_1 (= NR-PM_1 + BC) species (a) during the whole sampling period and (b) as a function of the PM_1 mass concentration (μg m^{-3}) bins (left). The right axis in (b) shows the accumulated data number in each bin. The organics were decomposed into primary oganic aerosol (POA) and secondary organic aerosol (SOA) using PMF (section 3.4).

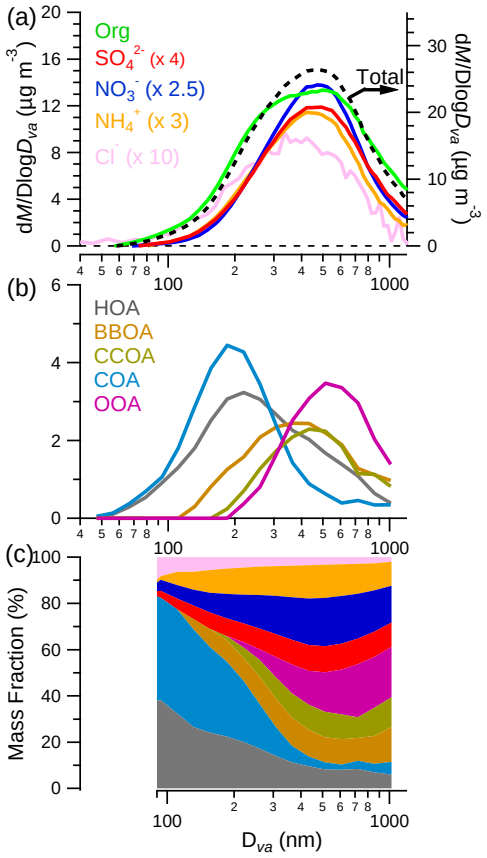

1287

1288 Fig. 3 The size distributions of (a) NR-PM_1 species, (b) organic components, and mass

1289 contribution of all species to NR-PM_1.

1290

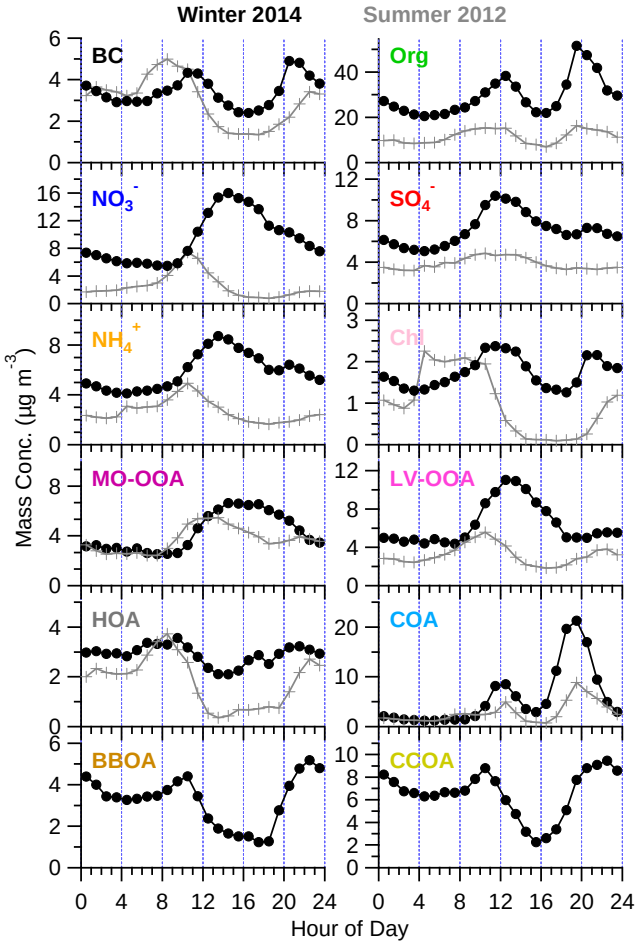

Fig. 4 The diurnal variation of PM_1 species during winter 2013/2014 and summer 2012.

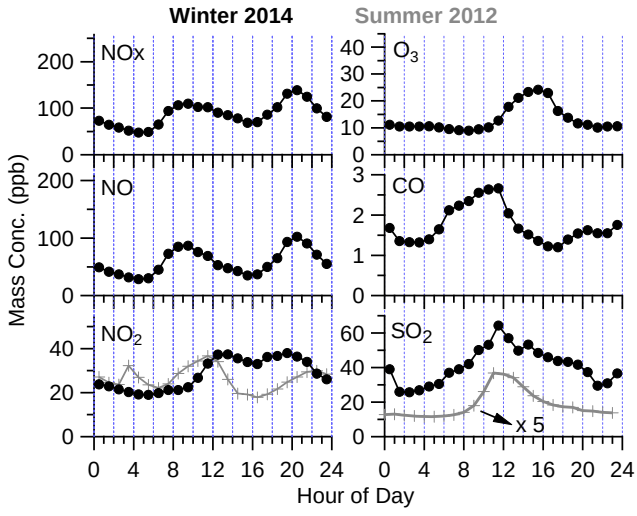

Fig. 5 The diurnal variations of gas species downloaded from MEP-China station during winter 2013/2014 and summer 2012.

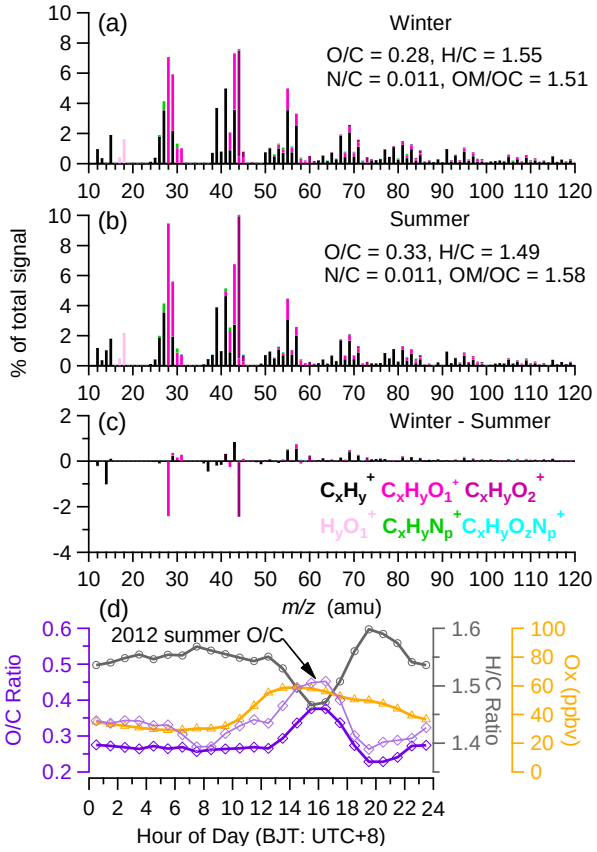

Fig. 6 The average HR-MS and elemental ratios of organics for (a) this study, (b) summer 2012, (c) the HR-MS difference between this study and summer 2012, and (d) the diurnal variations of elemental ratios and odd oxygen ($Ox = NO_2 + O_3$).

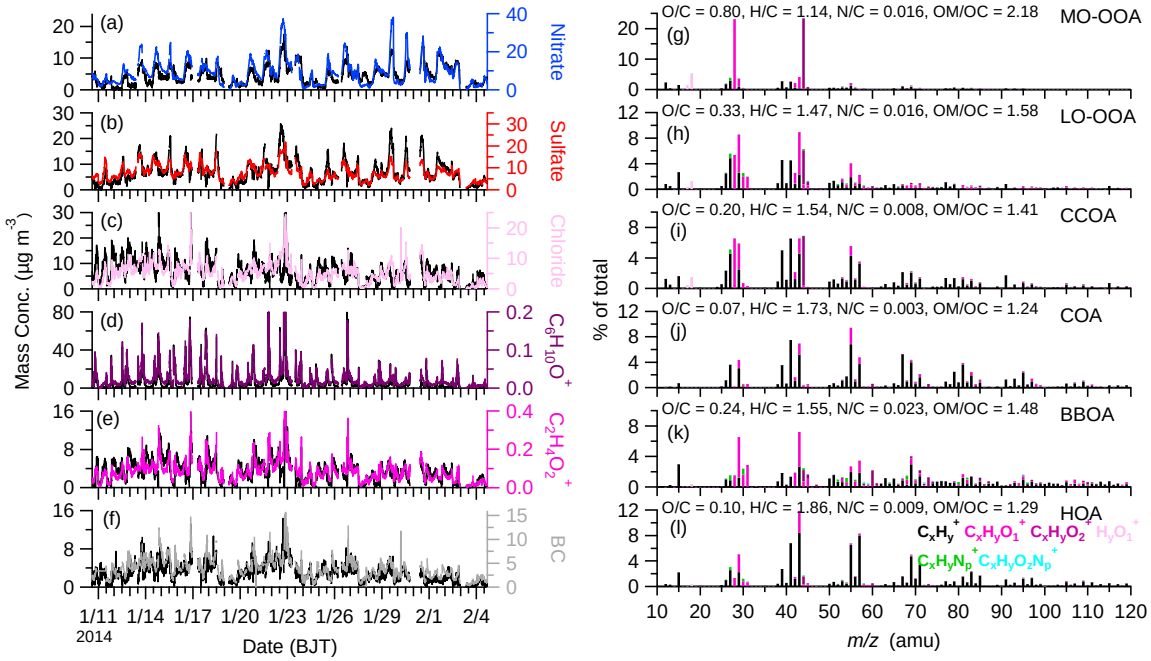

Fig. 7 The PMF results of time series (a – f) and HR-MS (g – l) for each component. The temporal variations of different tracers are also present for supporting each component.

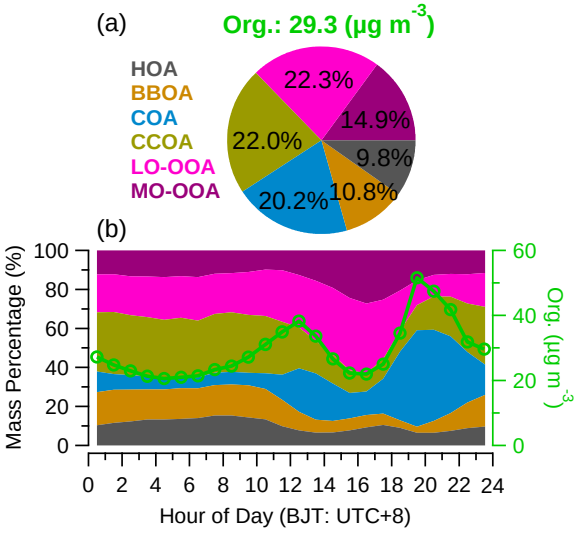

Fig. 8 (a) The average mass concentration of organics and mass contributions of organic components to organics, and (b) the diurnal variations of organic components and organics.

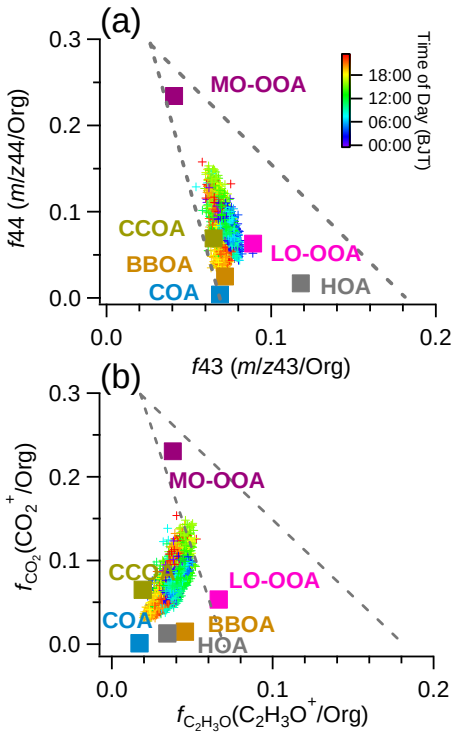

Fig. 9 Scatterplots of (a) *f*44 *vs.* *f*43 and (b) fCO_2^+ *vs.* $fC_2H_3O^+$. The cross dots correspond to measured OA data points are colored by time of the day. The corresponding values of the six OA factors identified in this study are also shown.

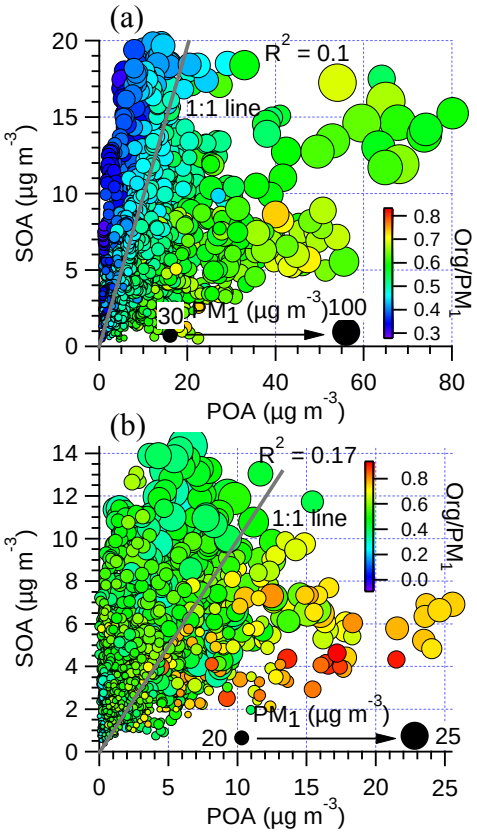

Fig. 10 The scatter plot of SOA and POA colored by the ratio of Org/PM_1 and sized by the mass concentration of PM_1 for (a) winter 2013/2014 and (b) summer 2012.

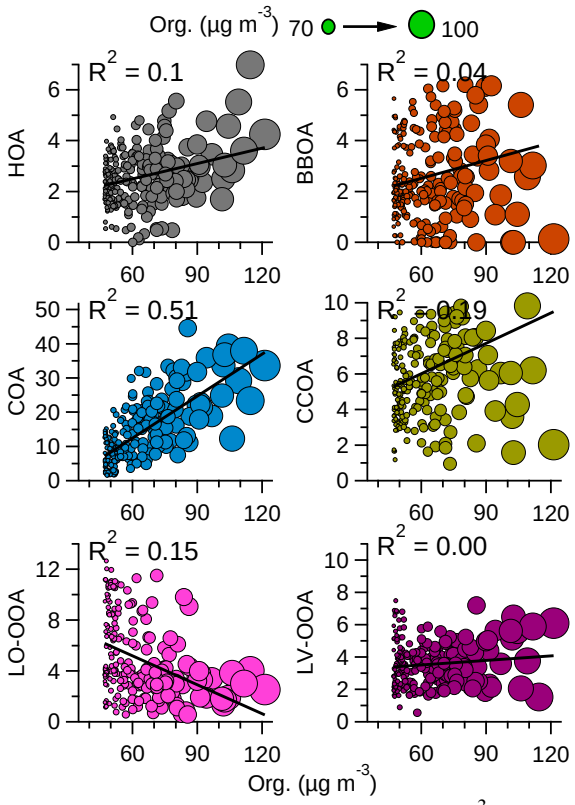

Fig. 11 The scatter plots of each organic component (µg m^{-3}) versus organics during haze periods (definite as organics > 43 µg m^{-3} (Org_avg + 1σ))

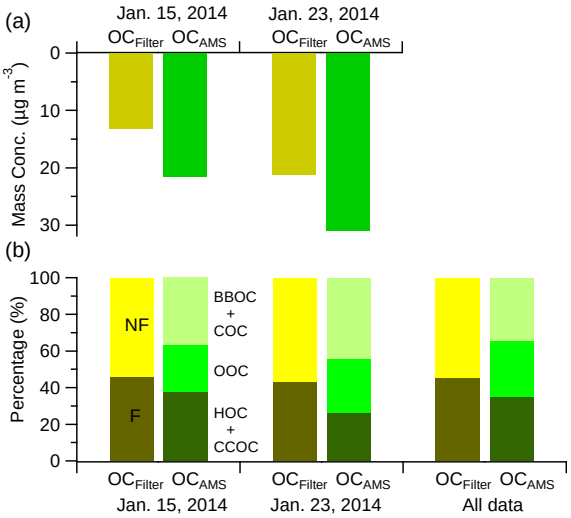

Fig. 12 The comparisons of (a) OC concentration measured by filter sample (OC_{Filter}) and AMS (OC_{AMS}) on Jan. 15 and 23, 2014 and (b) the non-fossil (NF) and fossil (F) carbon fraction measured by ^{14}C and OC components in AMS.

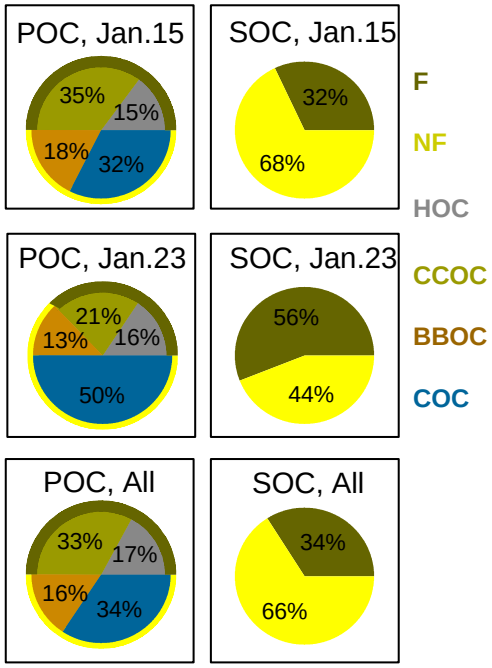

1332

1333 Fig. 13 The non-fossil (NF) and fossil (F) carbon fraction in POC and SOC during Jan.

1334 15, Jan. 23 and all data of AMS.

1335

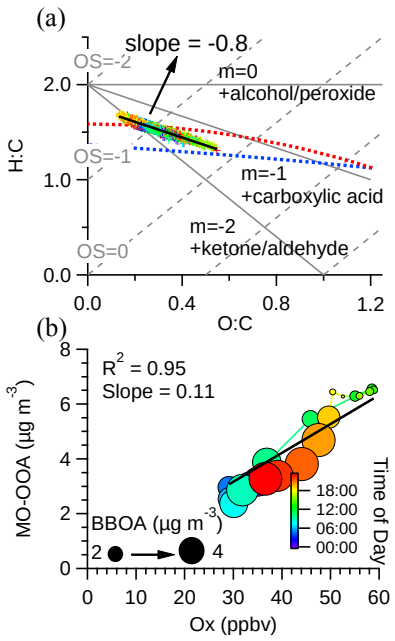

Fig. 14 (a) Van Krevelen diagram for OA and (b) scatter plot of MO-OOA *vs.* O_x (the sum of O_3 and NO_2) with linear fit and colored by time of day.